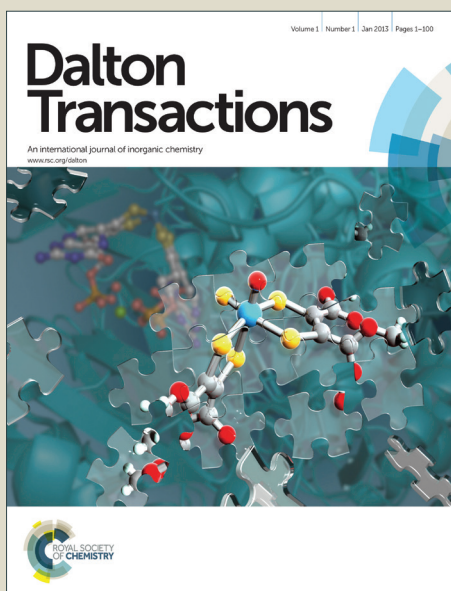


# Dalton Transactions

Accepted Manuscript



This article can be cited before page numbers have been issued, to do this please use: X. Fu, D. Liu, Y. Lin, W. Hu, Z. Mao and X. Le, *Dalton Trans.*, 2014, DOI: 10.1039/C3DT53577K.



This is an *Accepted Manuscript*, which has been through the Royal Society of Chemistry peer review process and has been accepted for publication.

*Accepted Manuscripts* are published online shortly after acceptance, before technical editing, formatting and proof reading. Using this free service, authors can make their results available to the community, in citable form, before we publish the edited article. We will replace this *Accepted Manuscript* with the edited and formatted *Advance Article* as soon as it is available.

You can find more information about *Accepted Manuscripts* in the [Information for Authors](#).

Please note that technical editing may introduce minor changes to the text and/or graphics, which may alter content. The journal's standard [Terms & Conditions](#) and the [Ethical guidelines](#) still apply. In no event shall the Royal Society of Chemistry be held responsible for any errors or omissions in this *Accepted Manuscript* or any consequences arising from the use of any information it contains.

# Water-soluble DNA minor groove binders as potential chemotherapeutic agents: Synthesis, characterization, DNA binding and cleavage, antioxidation, cytotoxicity and HSA interactions

Xia-Bing Fu,<sup>a</sup> Dan-Dan Liu,<sup>a</sup> Yuan Lin,<sup>a</sup> Wei Hu,<sup>a</sup> Zong-Wan Mao<sup>ac</sup> and Xue-Yi Le<sup>\*ab</sup>

<sup>a</sup> Department of Applied Chemistry, South China Agricultural University, Guangzhou 510642, PR China

<sup>b</sup> Institute of Biomaterial, South China Agricultural University, Guangzhou 510642, PR China

<sup>c</sup> School of Chemistry and Chemical Engineering, Sun yat-sen University, Guangzhou 510275, PR China

**Abstract:** Two new water-soluble copper(II)-dipeptide complexes: [Cu(glygly)(PyTA)]ClO<sub>4</sub>·1.5H<sub>2</sub>O (**1**) and [Cu(glygly)(PzTA)]ClO<sub>4</sub>·1.5H<sub>2</sub>O (**2**) (glygly = glycylglycine anion, PyTA = 2,4-diamino-6-(2'-pyridyl)-1,3,5-triazine and PzTA = 2,4-diamino-6-(2'-pyrazino)-1,3,5-triazine), utilizing two interrelated DNA base-like ligands (PyTA and PzTA), have been synthesized and characterized. The structure elucidation for **1** performed by single crystal X-ray diffraction shows a one dimensional chain conformation in which the central copper ions arrange in five-coordinate distorted square-pyramidal geometry. Spectroscopic titration, viscosity and electrophoresis measurements revealed that the complexes bound to DNA via an outside groove binding mode, and cleaved pBR322 DNA efficiently in the presence of ascorbate, probably via an oxidative mechanism in the involvement of ·OH and ·O<sub>2</sub><sup>-</sup>. Notably, the complexes exhibited considerable in vitro cytotoxicity against four human carcinoma cell lines (HepG2, HeLa, A549 and U87) with IC<sub>50</sub> values varying from 41.68 to 159.17 μM, in addition to their excellent SOD mimics (IC<sub>50</sub> ~ 0.091 and 0.114 μM). Besides, multispectroscopic evidence suggested their HSA-binding at the cavity containing Trp-214 in subdomain IIA with moderate affinity, mainly via the hydrophobic interaction. Further, the molecular docking technique utilized for ascertaining the mechanism and mode of action towards DNA and HSA theoretically verified the experiment results.

**Keywords:** DAT derivatives; DNA minor groove; SOD mimics; Anticancer activity; HSA binding; Molecular docking

## Introduction

The clinical application of cisplatin for treating most aggressive solid tumors pioneered the extensive researches of related platinum based reagents as the antitumor drugs.<sup>1</sup> Almost all clinical agents including cisplatin and related

platinum-based anticancer drugs act by covalently binding to the purine bases of DNA and then inducing severe DNA distortions (e.g. kink, or significant unwinding of the helices), thereby interdicting cellular replication and growth of tumor cells.<sup>2</sup> Despite their excellence in broad cytotoxicity, the clinical values are severely affected by their serious side effects, such as general toxicity and acquired drug resistance.<sup>3</sup> Therefore, it is imperative for chemists to develop the ideal anticancer agents not only with good water-solubility and accessible clinical value but also bringing fewer side effects, preferably non-covalently binding. Hence, much attention has been focused on transition metal complexes for their ability to cleave DNA by non-covalently binding under physiological conditions and low toxicity.<sup>4-7</sup> Among the various metal ion copper is an attractive prospect, being a bioessential trace element which plays a vital role in biological processes such as electron transfer, oxygen transport and endogenous oxidative DNA damage associated with aging and cancer.<sup>8,9</sup> Herein, copper-based hydrolytic cleavage reagents with better applications at the cellular level could be preference as chemotherapy agents.

Triazines with a special structure of aromatic heterocycles can bind to biological enzymes or receptors via hydrogen bonds, coordinate to metallic ion, and produce hydrophobic and  $\pi$ - $\pi$  conjugate interactions.<sup>10</sup> In addition, triazines and biological ligands, such as purine base, pyrimidine base and imidazole are very similar in structure, thus can easily interact with biological polymer (DNA, RNA, proteins, etc.) in the body. Therefore, triazines and its derivatives have a wide range of biological activities, such as antibacteria,<sup>11</sup> antitrypanosome,<sup>12</sup> antitumor,<sup>13</sup> antiretrovirus,<sup>14</sup> antagonism,<sup>15</sup> inhibition of sorbitol dehydrogenase,<sup>16</sup> adjust the estrogen receptor.<sup>17</sup> In recent years, diamino-s-triazine (DAT) derivatives have attracted much attention for their prominent anti-angiogenesis and antitumor activity.<sup>18</sup> DAT derivatives based metal complexes used as a hydrogen bond donors or auxiliary ligand of receptors can non-covalently bind to a specific base sequence of DNA groove through the hydrogen bonds between -NH<sub>2</sub> of DAT and DNA bases.<sup>19</sup> This specific groove binding, usually in the A-T enrichment region<sup>20</sup>, brings about some biological activity like antiprotozoan, antibacteria, antiviral and antitumor in particular<sup>21</sup>, which is applied to the molecular design of nucleic acid recognition reagents and anticancer drugs. Duong and coworkers obtained 2,4-diamino-6-(2'-pyridyl/pyrazinyl/pyrimidyl)-1,3,5-triazine based Ag(I) and Pd(II) complexes with supramolecular structure.<sup>22</sup> Ma et al. reported the 2-amino-4-anilino-6-(2'-pyridyl)-1,3,5-triazine based ruthenium (II) and rhenium (I) complexes, which target a A-T rich sequence in the DNA minor groove through the -NH<sub>2</sub> forming a wide range of hydrogen bonds network.<sup>23</sup> However, it is a pity that DAT derivatives based copper complexes are still rarely reported. On the other hand,

Copper(II)-peptide complexes may be regarded as models for both protein-DNA and antitumor agent-DNA interactions, since peptides are the basic structural units of proteins that recognize a specific base sequence of DNA.<sup>24</sup>

Based on the above consideration, it was thought necessary and worthwhile to assess the pharmacological properties of such DAT derivatives based copper complexes containing peptides. In this paper, two new water-soluble DAT derivatives based copper(II)-dipeptide complexes: [Cu(glygly)(PyTA)]ClO<sub>4</sub>·1.5H<sub>2</sub>O (**1**) and [Cu(glygly)(PzTA)]ClO<sub>4</sub>·1.5H<sub>2</sub>O (**2**) [PyTA = 2,4-diamino-6-(2'-pyridyl)-1,3,5-triazine, PzTA = 2,4-diamino-6-(2'-pyrazino)-1,3,5-triazine, glygly = glycylglycine anion], have been synthesized and characterized. The DNA binding and cleavage properties of the complexes were explored by employing various spectral methods, viscosity and electrophoresis measurements. The SOD-like activities of the complexes were evaluated using the photoreduction of nitroblue tetrazolium (NBT) assays, and their in vitro antitumor activities were assessed by MTT assays, against four human carcinoma cell lines (HepG2, HeLa, A549 and U87). Besides, the protein binding behavior in vitro was monitored by multispectroscopic techniques, using HSA as a model protein. Further, the molecular docking technique was also utilized to ascertain the mechanism and action mode of the complexes towards DNA and HSA. We hope the obtained results may contribute to the rational molecular design of DNA groove targeting reagents with high affinity and specificity as potential antitumor chemotherapeutic agents, as well as elucidate valuable information to understand their specific delivery at the active site of action, besides providing the pharmacological behaviors in vitro.

## Experimental

### Materials and instruments

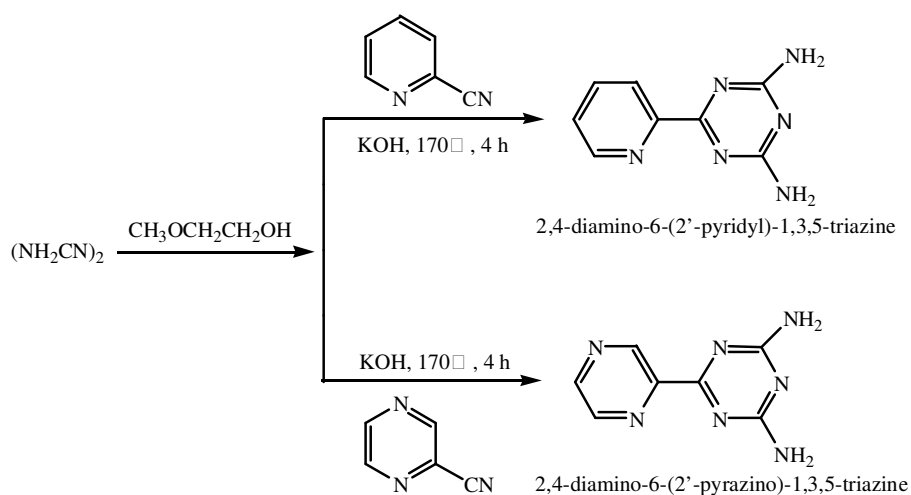
All reagents and chemicals of analytical reagent grade were commercially purchased and used as received. Glycylglycine (glygly), Tris(hydroxymethyl)aminomethane, ethidium bromide (EB), nitroblue tetrazolium (NBT) and Calf thymus (CT)-DNA were obtained from Sigma (USA), plasmid DNA pBR322 and loading buffer (10X) from Fermentas (Lithuania), and human serum albumin (HSA) from Wako (Japan). Human carcinoma cell lines of HepG2 (hepatocellular), HeLa (cervical), A549 (pulmonary) and U87 (cerebral glioma) were obtained from Laboratory Animal Center of Sun yat-sen university. Doubly distilled water was used as the solvent throughout the experiments. The stock solution of CT-DNA was prepared in 5 mM Tris-HCl/50 mM NaCl buffer at pH 7.2, and the stock solution of HSA was

prepared by dissolving the solid HSA in 0.05 M Tris-HCl/0.15 M NaCl buffer at pH 7.4. All stock solutions were stored at 4 °C and used within 3 days.

Elemental analyses (C, H, N) were determined using a Vario EL elemental analyzer (Elementar, Germany). Infrared spectra (KBr pellets) were recorded on a Nicolet ACATAR 360 FT-IR spectrometer (Nicolet, USA) in the range 4000 – 400  $\text{cm}^{-1}$ . Molar conductivities were measured on a DDS-11A digital conductometer (LeiCi, China) at room temperature in  $1.0 \times 10^{-3}$  M aqueous solution. ESI-MS was processed on a API4000 (AB Sciex, USA). Electronic spectra were carried out on a Pharmacia 2550 UV-Vis spectrophotometer (Shimadzu, Japan). Emission spectra were performed on a Hitachi RF-4500 fluorescence spectrophotometer (Hitachi, Japan) equipped with a thermostatic bath. Circular dichroism spectroscopy were taken on a Chirascan CD spectropolarimeter (Applied Photophysics, UK) at room temperature. The agarose gel electrophoresis was conducted on a Powerpac Universal-JY200C (LiuYi, Beijing), and the gel imaging and densitometric analysis were assessed using BIO-RAD Laboratories-Seqrate imaging and Gel Documentation Systems.

### Synthesis of ligands and corresponding copper(II) complexes

**Synthesis of the ligands (PyTA and PzTA).** The ligands were prepared on the basis of the established method for the preparation of 2,4-diamino-s-triazine<sup>25</sup>, by the reactions of 2-cyano-pyridyl or 2-cyano-pyrazine with dicyandiamide dissolved in 2-methoxyethanol in the presence of KOH, as shown in **Scheme 1**.



**Scheme 1.** Synthesis of the ligands PyTA and PzTA

**Synthesis of [Cu(glygly)(PyTA)]ClO<sub>4</sub>·1.5H<sub>2</sub>O (1).** To an aqueous solution (5 mL) of glygly (0.066 g, 0.5 mmol) and NaOH (0.020 g, 0.5 mmol) was added an aq. soln. of Cu(ClO<sub>4</sub>)<sub>2</sub>·6H<sub>2</sub>O (0.186 g, 0.5 mmol) with stirring, followed by the addition of PyTA (0.094 g, 0.5 mmol) in ethanol (20 ml). The resulting solution was stirred for ca. 3 h at 60 °C. After filtration, blue block crystals suitable for X-ray diffraction were obtained by slow evaporation of the filtrate after several days at room temperature, which were collected by filtration, washed with ice cold ethanol (yield: 0.112 g, 44%). Anal. Calc. for C<sub>12</sub>H<sub>19</sub>ClN<sub>8</sub>O<sub>8.5</sub>Cu (%): C, 28.30; H, 3.56; N, 22.00. Found: C, 28.12; H, 3.45; N, 21.90. IR (KBr, cm<sup>-1</sup>): 3321 ν(NH<sub>2</sub> + H<sub>2</sub>O), 1618 ν<sub>as</sub>(-COO<sup>-</sup>), 1589 ν(C=N), 1384 ν<sub>s</sub>(-COO<sup>-</sup>), 1090 ν(Cl-O), 789 ν(=CH), 538 ν(Cu-O), 432 ν(Cu-N). UV-Vis absorption (H<sub>2</sub>O), λ<sub>max</sub>/nm (ε/M<sup>-1</sup> cm<sup>-1</sup>): 203.4 (34634), 276.2 (7143), and 647.4 (69.12). Molar Conductance, A<sub>M</sub> (1 × 10<sup>-3</sup> M, H<sub>2</sub>O): 109.3 S<sup>-1</sup> cm<sup>2</sup> mol<sup>-1</sup>. ESI-MS (m/z, H<sub>2</sub>O): 383.1, [Cu(glygly)(PyTA)]<sup>+</sup>

**Synthesis of [Cu(glygly)(PzTA)]ClO<sub>4</sub>·1.5H<sub>2</sub>O (2).** To an aqueous solution (5 mL) of glygly (0.066 g, 0.5 mmol) and Cu(ClO<sub>4</sub>)<sub>2</sub>·6H<sub>2</sub>O (0.186 g, 0.5 mmol) was added an ethanol solution (20mL) of PzTA (0.0095 g, 0.5 mmol) with stirring. The stirring was continued for ca. 3 h at 60 °C. The resulting blue solution was filtered off and allowed to evaporate for a few days at room temperature until blue colored crystals formed. The crystals were collected by filtration, washed with ice cold ethanol. (yield: 0.123 g, 48%). Anal. Calc. for C<sub>11</sub>H<sub>19</sub>ClN<sub>9</sub>O<sub>8.5</sub>Cu (%): C, 25.89; H, 3.36; N, 24.70. Found: C, 25.97; H, 3.18; N, 24.70. IR (KBr, cm<sup>-1</sup>): 3323 ν(NH<sub>2</sub> + H<sub>2</sub>O), 1631 ν<sub>as</sub>(-COO<sup>-</sup>), 1517 ν(C=N), 1378 ν<sub>s</sub>(-COO<sup>-</sup>), 1092 ν(Cl-O), 803 ν(=CH), 583 ν(Cu-O), 471 ν(Cu-N). UV-vis absorption (H<sub>2</sub>O), λ<sub>max</sub>/nm (ε/M<sup>-1</sup> cm<sup>-1</sup>): 210.6 (36581), 274.4 (11195), and 648.8 (58.67). Molar Conductance, A<sub>M</sub> (1 × 10<sup>-3</sup> M, H<sub>2</sub>O): 105.8 S<sup>-1</sup> cm<sup>2</sup> mol<sup>-1</sup>. ESI-MS (m/z, H<sub>2</sub>O): 385.1, [Cu(glygly)(PzTA)]<sup>+</sup>

*Caution!* Perchlorate salts of metal complexes with organic ligands are potentially explosive and therefore should be prepared in small quantities and handled carefully.

**X-ray crystallography.** Single crystal X-ray diffraction data of complex **1** were collected on a Bruker SMART 1000 CCD diffractometer at 298(2) K using graphite monochromated Mo-Kα radiation (λ = 0.71073 Å) with the ω-2θ scan technique. The collected data were reduced by using the SAINT program. The structure was solved by direct methods and refined with the full-matrix least-squares techniques on F<sup>2</sup> using the SHELXL-97.<sup>26</sup> Anisotropic thermal parameters were assigned to all non-hydrogen atoms and the remaining hydrogen atoms were added theoretically, and refined as riding atoms with fixed isotropic thermal parameters. The crystallographic data and structure refinement parameters are summarized in **Table 1**, and the selected bond distances and angles are listed in **Table 2**.

**Table 1** Selected crystallographic data for complex **1**

Parameter	
Formula	C <sub>12</sub> H <sub>19</sub> ClCuN <sub>8</sub> O <sub>8.5</sub>
Formula weight	510.34
Crystal system	Monoclinic
Space group	P21/c
<i>a</i> (Å)	7.4245(11)
<i>b</i> (Å)	14.9800(2)
<i>c</i> (Å)	17.2929(18)
$\alpha$ (°)	90
$\beta$ (°)	104.992
$\gamma$ (°)	90
<i>V</i> (Å <sup>3</sup> )	1857.8(4)
<i>Z</i>	2
<i>D</i> <sub>calc</sub> (g cm <sup>-3</sup> )	1.825
$\mu$ (Mo <i>K</i> $\alpha$ ) (mm <sup>-1</sup> )	1.387
<i>F</i> (000)	1044
Crystal size (mm <sup>3</sup> )	0.43 × 0.41 × 0.38
Temp (K)	293(2)
Measured reflns	8462
Unique reflns	3235
$\theta$ Range for data collection (°)	2.44 ~ 25.00
No. of data/parameters/restraints	3235/283/0
Index ranges	-8 ≤ <i>h</i> ≤ 8, -17 ≤ <i>k</i> ≤ 17, -20 ≤ <i>l</i> ≤ 11
<i>R</i> (int)	0.0177
Goodness-of-fit on <i>F</i> <sup>2</sup>	1.063
Final <i>R</i> indices [ <i>I</i> > 2 $\sigma$ ( <i>I</i> )]	<i>R</i> <sub>1</sub> = 0.0488, <i>wR</i> <sub>2</sub> = 0.1233
<i>R</i> indices (all data)	<i>R</i> <sub>1</sub> = 0.0559, <i>wR</i> <sub>2</sub> = 0.1273
Largest diff. peak and hole (e Å <sup>-3</sup> )	1.733 and -1.066

**Table 2** Selected bond lengths (Å) and angles (°) for complex **1**

bond lengths (Å)		bond angles (°)	
Cu1–O2	2.048(3)	O2–Cu1–N1	95.15(12)
Cu1–N1	2.001(3)	O2–Cu1–N4	152.63(12)
Cu1–N4	2.017(3)	O2–Cu1–N7	81.06(12)
Cu1–N7	1.994(3)	O1WA–Cu1–O2	95.93(11)
Cu1–O1WA	2.143(3)	N1–Cu1–N4	81.63(13)
		N1–Cu1–N7	171.65(14)
		O1WA–Cu1–N1	96.90(12)
		N4–Cu1–N7	98.29(13)
		O1WA–Cu1–N4	111.44(12)
		O1WA–Cu1–N7	90.92(13)

### DNA-binding and cleavage experiments

**UV spectroscopy.** Electronic absorption spectra were determined in the range of 190 – 400 nm by increasing amounts of CT-DNA (to give a final concentrations of 35.70  $\mu\text{M}$ ) to the complexes (50  $\mu\text{M}$ ) in 5 mM Tris-HCl/50 mM NaCl buffer (pH 7.2) at room temperature. In the reference cell, simultaneously, a DNA blank was also placed so as to eliminate any absorbance due to DNA at the measured wavelength. Each sample was kept for 10 min to equilibrium before recording its spectrum.

**Fluorescence spectroscopy.** Emission spectra were recorded between 530 and 700 nm at room temperature with the excitation wavelength set at 525 nm, by the addition of the copper(II) complex solution ( $1.0 \times 10^{-2}$  M) (to give a final concentrations of 117.65  $\mu\text{M}$ ) to a sample containing 8  $\mu\text{M}$  EB and 10  $\mu\text{M}$  CT-DNA in Tris-HCl buffer (pH 7.2). For every addition, the sample was shaken and allowed to keep for 10 min, and then the fluorescence emission spectra were recorded.

**CD spectroscopy.** CD spectra of CT-DNA (100  $\mu\text{M}$ ) were determined at room temperature by increasing [Complex]/[CT-DNA] ratio ( $r = 0, 0.2, 0.4, 0.6, 0.8, 1.0$ ) in 5 mM Tris-HCl/50 mM NaCl buffer (pH 7.2). Each sample solution was scanned in the range of 200 – 320 nm, and its final CD spectrum was generated after averaging three scans and subtracting the buffer background.

**Viscosity measurement.** The viscosity of CT-DNA (200  $\mu\text{M}$ ) in the absence and presence of the complexes (with the [Complex]/[CT-DNA] ratio of 0, 0.05, 0.10, 0.15, 0.20, 0.25, 0.30 and 0.35) in Tris-HCl buffer (pH 7.2) was measured using an Ostwald Viscometer at 29 ( $\pm 0.1$ )  $^{\circ}\text{C}$ . Each sample was measured in triplicate for accuracy, and an average flow time was determined. Data were presented as  $(\eta/\eta_0)^{1/3}$  versus [Complex]/[DNA], where  $\eta_0$  and  $\eta$  represent the viscosity of CT-DNA solution in the absence and presence of the complexes, respectively. Viscosity values were calculated according to the relation  $\eta = (t-t_0)/t_0$ , where  $t$  was the flow time of samples containing CT-DNA and  $t_0$  that of the buffer alone.

**DNA cleavage experiments.** The DNA cleavage activity of the complexes was monitored using agarose gel electrophoresis experiments performed as follows: pBR 322 DNA (200 ng), ascorbate (0.5 mM), and tested compounds [Cu(ClO<sub>4</sub>)<sub>2</sub> (20  $\mu\text{M}$ ), PyTA/PZTA (20  $\mu\text{M}$ ), glygly (20  $\mu\text{M}$ ), titled complexes (5 – 20  $\mu\text{M}$ )] in Tris-HCl buffer (pH 7.2) to yield a total volume of 20  $\mu\text{L}$ . The control experiments were carried out using titled complexes (20  $\mu\text{M}$ ) in the absence of ascorbate (0.5 mM). The samples were incubated at 37  $^{\circ}\text{C}$  for 3 h, and then loading buffer was added. The

resulting solutions were electrophoresed for 40 min at 120 V on 0.8% agarose gels containing 4 – 5  $\mu\text{L}$  goldview in TBE buffer ( $4.5 \times 10^{-2}$  M Tris +  $4.5 \times 10^{-2}$  M  $\text{H}_3\text{BO}_3$  +  $10^{-3}$  M EDTA, pH = 8.0), and the gel bands were visualized and photographed on a BIO-RAD Laboratories-Stratagene gel imaging system. The cleavage mechanistic investigation was carried out in the presence of typical radical scavengers such as hydroxyl radical scavengers [dimethyl sulfoxide (DMSO), tert-butyl alcohol, and ethanol], a singlet oxygen quencher [2,2,6,6-tetramethylpiperidine (TMP) and sodium azide ( $\text{NaN}_3$ )] and a superoxide anion radical scavenger [superoxide dismutase (SOD)]. Each sample was analyzed according to the procedure described above.

### Determination of the superoxide dismutase activity

The superoxide dismutase activities of the complexes were assayed using the modified nitroblue tetrazolium (NBT) photoreduction,<sup>27</sup> and performed at  $25 (\pm 0.1) ^\circ\text{C}$  as follows: solutions containing the tested complexes ( $0.05 \times 10^{-6}$  –  $0.8 \times 10^{-6}$  M), NBT ( $9.32 \times 10^{-5}$  M), riboflavin ( $6.80 \times 10^{-6}$  M), and tetramethyl-ethylenediamine ( $1.0 \times 10^{-4}$  M) in phosphate buffer at pH 7.8 were used. The NBT reduction rates were measured in the absence and presence of the investigated complexes for 7 min. The SOD mimetic activities of the complexes in aqueous solution were evaluated from the absorbance decrease at 560 nm comparing to the blank reaction solution (without the complexes). The concentrations of the complexes required to yield 50% inhibition of NBT reduction (the  $\text{IC}_{50}$  values) were determined from a plot of percentage inhibition versus copper complexes concentration. Each final results for  $\text{IC}_{50}$  values are the average of three independent determinations.

### Cytotoxic activity assays (MTT)

Four different human tumour cell lines were subjected to cytotoxicity tests in vitro: HepG2 (hepatocellular), HeLa (cervical), A549 (pulmonary) and U87 (cerebral glioma). Standard MTT assay procedures<sup>28</sup> were used for testifying cytotoxicity. A cell suspension (100  $\mu\text{L}$ ) was seeded into 96-well microtiter plates ( $1 \times 10^4$  cells per well) and incubated overnight at  $37 ^\circ\text{C}$  in a 5%  $\text{CO}_2$  incubator. The tested compounds were dissolved in DMSO and diluted with RPMI 1640 to the required concentrations (ranging from 3.125 to 200  $\mu\text{M}$ ) prior to use. Control wells were prepared by addition of culture medium (100  $\mu\text{L}$ ). Wells containing culture medium without cells were used as blanks. The plates were incubated at  $37 ^\circ\text{C}$  in a 5%  $\text{CO}_2$  incubator for 48 h. Then each well was loaded with stock MTT (3-(4,5-dimethylthiazol-2-yl)-2,5-diphenyltetrazolium bromide) dye solution (20  $\mu\text{L}$ , 5 mg/mL) and incubated for 4 h at

37 °C. The formed formazan crystals were then dissolved in 100  $\mu$ L DMSO, and the optical density of each well was then measured at 570 nm on a Tecan Infinite F200 plate reader (Switzerland). The  $IC_{50}$  values were determined by plotting the percentage viability versus concentration on a logarithmic graph and reading off the control. Each experiment was repeated three times, and the final  $IC_{50}$  values were calculated by the average of triplicate experimental results.

### HSA binding experiments

**Fluorimetric experiments.** The protein binding studies were performed by fluorescence quenching titration experiments using human serum albumin as a model protein in 0.05 M Tris-HCl/0.15 M NaCl buffer (pH 7.4). A 3.0 mL portion of aqueous solution of HSA (10  $\mu$ M) was titrated by the complexes (to give a final concentration of 26.0  $\mu$ M). Each sample solution was shaken and allowed to keep for 5 min at the corresponding temperatures (300 K and 310 K), and then the fluorescence spectra were recorded with the excitation wavelength at 280 nm and emission at 342 nm. Simultaneously, the synchronous fluorescence spectra of the mixture solutions in the range of 300 – 500 nm were recorded, by setting  $\Delta\lambda = 60$  nm and  $\Delta\lambda = 15$  nm for tyrosine and tryptophan residues respectively. Moreover, 3D fluorescence spectra of HSA (10  $\mu$ M) in the absence and presence of the complexes (10  $\mu$ M) were performed in the range of 240 – 600 nm at room temperature.

**UV absorption spectra.** The UV absorption spectra of HSA (10  $\mu$ M) in 0.05 M Tris-HCl/0.15 M NaCl buffer (pH 7.4) in the absence and presence of increasing concentration of the complexes (ranging from 0 to 80  $\mu$ M) were obtained, together with the spectra of the complexes (10  $\mu$ M) alone.

**CD spectra.** CD spectra of HSA (1.5  $\mu$ M) before and after addition of increasing concentration of the complexes (3.0, 6.0, and 9.0  $\mu$ M) were recorded in the range of 200 – 260 nm, and the contents of different secondary structures of HSA were calculated from the spectral data.

### Molecular docking

Molecular docking was performed by using Autodock 4.2 program.<sup>29</sup> The PDB format of complex **1** was obtained by converting its CIF file using Mercury software. The crystal data of the B-DNA dodecamer d(CGCGAATTCGCG)<sub>2</sub> (PDB ID: 1BNA)<sup>6</sup> and HSA (PDB ID: 1H9Z)<sup>30</sup> were downloaded from the Protein Data Bank. The water molecules and the ligands were removed from the 1BNA and 1H9Z, and Gasteiger charges were added to the complex by

Autodock Tools (ADT) before performing docking calculations. The binding site was centered on the macromolecules (DNA/HSA) and a grid box was created with  $60 \times 60 \times 60$  points and a  $0.375 \text{ \AA}$  grid spacing in which almost the entire macromolecules involved. Docking simulations were performed using the classical Lamarckian genetic algorithm (LGA) and the lattice point search method. The runs of rigid docking operation were set 200, and each run was terminated after a maximum of 2500000 energy evaluations. In addition, the other parameters are the default parameters.

## Results and discussion

### Synthesis and characterization

The titled complexes were isolated by mixing stoichiometric amounts of glycylglycine with copper chloride dihydrate in 80% (v/v) ethanol-water solution, followed by reactions with PyTA and PzTA. The resulting complexes are stable towards air and moisture and readily soluble in aqueous solution. The complexes were characterized from elemental analysis, molar conductivity, IR, UV-Vis and ESI-MS data. The elemental analytical data cohere well with the molecular formula of the complexes, and the molar conductance values in aqueous solution ( $1 \times 10^{-3} \text{ M}$ ) at  $25 \text{ }^\circ\text{C}$  are within the scope of  $80 - 160 \text{ S cm}^2 \text{ mol}^{-1}$  suggesting their 1:1 electrolyte nature.<sup>31</sup> Besides, the ESI-MS for the complexes in methanol shows peaks at  $m/z = 383.1$  and  $385.1$ , matching exactly with the coordination cations  $[\text{Cu}(\text{glygly})(\text{PyTA})]^+$  and  $[\text{Cu}(\text{glygly})(\text{PzTA})]^+$  respectively. Further, the formulation of complex **1** was confirmed by determination of the X-ray crystal structure.

**Description of the crystal structure.** The single crystal X-ray analysis revealed that complex **1** crystallizes as a monoclinic crystal system with space group P21/c. An ORTEP view of the complex (**Fig. 1**) shows a polymeric structure for cation  $[\text{Cu}(\text{glygly})(\text{PyTA})]^+$ , where the central copper ion is in a N3O2 coordination environment arranged in a distorted square-pyramidal geometry, as evidenced by all the angles around which deviate from  $90^\circ$  and  $180^\circ$ , the distance from the axial atom O1W to basal plane ( $2.3716 \text{ \AA}$ ) which deviates from the O1W-Cu1 bond length ( $2.143 \text{ \AA}$ ), and the calculated Tau = 0.32 (Tau = 0.00 for standard square-pyramidal geometry, and Tau = 1.00 for standard trigonal bipyramid). The coordination basal plane around copper center is achieved by the bidentate PyTA ligand [Cu1-N1  $2.001(3) \text{ \AA}$  and Cu1-N4  $2.017(3) \text{ \AA}$ ] and the dipeptide through the carbonyl oxygen [Cu-O2  $2.048(3) \text{ \AA}$ ] and terminal amino nitrogen [Cu1-N7  $1.994(3) \text{ \AA}$ ], and the axial position is occupied by one carboxylate oxygen atom belonging to

the symmetrically related neighbouring dipeptide molecule [Cu1–O1WA 2.143(3) Å]. Thus each dipeptide molecule (glygly) links two copper atoms along a single screw axis (c axis), thereby producing an infinite one dimensional chain (–Cu–O–NO–Cu–O–NO–) structure. The PyTA or pyridine ring project parallelly in the same direction and stack on each other with average spacings of 5.508(2) Å and 5.314(2) Å, respectively. Furthermore, the Cu1–N1 distance is slightly shorter than the Cu1–N4 distances, indicating that the s-triazine nitrogen (N1) is more strongly coordinated to the metal center than the pyridine nitrogen (N4). On the other hand, the Cu–O<sub>carbonyl</sub> bond lengths exhibit smaller values than Cu–O<sub>carboxylate</sub>. The small bite angles of N(1)–Cu(1)–N(4) [81.65(13)°] and O2–Cu1–N7 [81.05(13)°] are primarily responsible for distortion from the regular square-pyramidal geometry. Whereas, the angles between N1–Cu1–N7, O2–Cu1–N1, O2–Cu1–N4 and N4–Cu1–N7 are 171.63(14)°, 95.14(12)°, 152.64(12)° and 98.27(13)°, respectively. The chelation of dipeptide through the amino N and the carbonyl O with the formation of a five-membered ring, an unusual metal coordination mode, similar to the reported copper-dipeptide complex [Cu(Gly-Gly)(ambzim)(H<sub>2</sub>O)]Cl·H<sub>2</sub>O.<sup>32</sup>

**Fig. 1**

The crystal packing is largely determined by alternate s-triazine-pyridine (a, 3.518 Å) and pyridine-s-triazine (b, 4.439 Å) ring-ring ( $\pi$ - $\pi$ ) stacking interactions (**Fig. 2a**) and an extensive network of hydrogen-bond interactions (**Fig. 2b**), involving interchain hydrogen bonds between the carboxylate oxygen of glygly and the hydrogen of pyridine [c1 and c2, C11–H11...O3 (2.56 Å)] maintaining the stability of the space structure, and intrachain hydrogen bonds between the terminal carboxylate oxygen and the amino hydrogen of dipeptide [d, N7–H7B... O1W (2.06 Å); e, N7–H7B...O3 (2.28 Å)], and between the carbonyl oxygen of dipeptide and the amino hydrogen of s-triazine [f, N5–H5B...O2 (2.14 Å)] maintaining the polymer chain structure. Therefore, the stereo packed structure was achieved by self-assembly through  $\pi$ - $\pi$  stacking and extensive hydrogen-bond interactions.

**Fig. 2**

**Infrared spectra.** The IR spectra of the complexes show a strong and wide band near 3320 cm<sup>-1</sup> attributed to the stretching vibrations of the water molecules and -NH<sub>2</sub> groups. The bands near 1618 and 1384 cm<sup>-1</sup> for **1** (1631 and 1378 cm<sup>-1</sup> for **2**) can be attributed, respectively, to asymmetric  $\nu_{as}$  (COO<sup>-</sup>) and symmetric  $\nu_s$  (COO<sup>-</sup>) stretching vibrations of

the coordinated carboxylate groups.<sup>33</sup> The difference values [ $\nu_{as}(\text{COO}^-) - \nu_s(\text{COO}^-)$ ] are greater than  $200\text{ cm}^{-1}$  indicating an asymmetric coordination mode of the carboxylate group, in agreement with the single crystal X-ray crystallography for complex **1**. In addition, the bands at  $1589$  and  $1517\text{ cm}^{-1}$  can be assigned to the ring stretching vibrations  $\nu(\text{C}=\text{N})$  of PyTA and PzTA, respectively, indicating that PyTA and PzTA were coordinated to the central Cu(II) ion. Besides, the band near  $1090\text{ cm}^{-1}$  can be ascribed to the  $\nu(\text{Cl}-\text{O})$  of  $\text{ClO}_4^-$ , and the bands at  $538$  and  $432\text{ cm}^{-1}$  for **1** ( $583$  and  $471\text{ cm}^{-1}$  for **2**) most likely belong to the  $\nu(\text{Cu}-\text{O})$  and  $\nu(\text{Cu}-\text{N})$ , respectively.<sup>6</sup>

**Electronic spectra.** The electronic absorption spectra of the complexes in aqueous solution exhibit three characteristic absorption bands with varied intensities and width. The intense and narrow bands ( $203.4\text{ nm}$  for **1**, and  $210.6\text{ nm}$  for **2**) can be assigned to  $n \rightarrow \pi^*$  transition of dipeptide (glygly), and the medium and broad bands ( $275.6\text{ nm}$  for **1**, and  $274.4\text{ nm}$  for **2**) to the intra-ligand LMCT transitions ( $\pi \rightarrow \pi^*$ ) of PyTA and PzTA. Moreover, the weak and low energy bands ( $647.4\text{ nm}$  for **1**, and  $648.8\text{ nm}$  for **2**) can be attributed to  ${}^2B_{1g} \rightarrow {}^2B_{2g}$  transitions of the central Cu(II) ion, typical for a distorted square-pyramidal geometry.<sup>34</sup>

Based on the above characterization results, we can safely deduce that **2** has a similar structure to **1**. In addition, in the solution, there may be the following ionization equilibrium for the complexes:  $[\text{Cu}(\text{glygly})(\text{PxTA})]_n^+ + n\text{ H}_2\text{O} = n[\text{Cu}(\text{H}_2\text{O})(\text{glygly})(\text{PxTA})]_n^+$  ( $x = y/z$ ).

### DNA-binding properties

**Electronic absorption titration.** Electronic absorption spectrum is one of the most universally employed methods in examining the binding mode and extent of complexes to DNA by the changes in the absorbance and shift in the wavelength. The absorption titration curves of the complexes in the range of  $190 - 400\text{ nm}$  are presented in **Fig. 3**. Upon addition of increasing amounts of CT-DNA to the complexes, an increase in the absorption intensity (hyperchromism) of LMCT absorption peak with a visible blue shift (**1**,  $277 \rightarrow 272\text{ nm}$ ; **2**,  $276 \rightarrow 273\text{ nm}$ ) are observed. The observations may indicate that there are interactions between DNA and the complexes via a non-classical intercalation, probably electrostatic and/or groove binding modes, leading to small perturbations.<sup>35,36</sup> Hyperchromism with blue shift in absorbance could be due to the external contact (surface binding) of the complexes with the duplex via hydrogen-bond interactions of  $-\text{NH}_2$  and  $-\text{COO}^-$  of dipeptide (glygly) and uncoordinated  $-\text{NH}_2$  of DAT group with functional groups positioned on the edge of DNA bases which are accessible both in the major and minor grooves, or

attributed to strong binding of the complexes to the phosphate backbone of DNA helix via electrostatic interactions.<sup>6,37,38</sup> DAT group ( $-\text{NH}_2$ ) and dipeptide ( $-\text{NH}_2$  and  $-\text{COO}^-$ ) used as hydrogen bond donors can non-covalently bind to H-bond acceptor groups (the purine N(3) and pyrimidine O(2) at the floor of the groove walls) through the hydrogen bonds.<sup>19</sup> These results were further validated by molecular docking studies. To assess the binding ability between the complexes and CT-DNA, the intrinsic binding constants  $K_b$  were calculated using the following equation:<sup>39</sup>

$$[\text{DNA}]/(\varepsilon_a - \varepsilon_f) = [\text{DNA}]/(\varepsilon_b - \varepsilon_f) + 1/K_b(\varepsilon_b - \varepsilon_f) \quad (1)$$

where  $K_b$  is the ratio of the slope to the intercept (respective insets of Fig. 3) and found to be  $4.75 \times 10^4 \text{ M}^{-1}$  for **1** and  $6.04 \times 10^3 \text{ M}^{-1}$  for **2**, following the order: **1** > **2**. The  $K_b$  values suggest moderate binding ability of the complexes to CT-DNA, and **2** shows a lower binding affinity for CT-DNA in comparison to **1** due to the larger steric hindrance.

**Fig. 3**

**Ethidium bromide displacement assay.** No luminescence is observed for the complexes at room temperature in aqueous solution, and therefore competitive binding assays were carried out using ethidium bromide (EB) as a probe, to further clarify the DNA-binding of the complexes. EB emits intense fluorescent in the presence of DNA due to its strong intercalation between the adjacent DNA base pairs, which could be quenched after the addition of a second DNA-binding molecule by either replacing the EB and/or by accepting the excited-state electron of the EB through a photoelectron transfer mechanism.<sup>40,41</sup> An appreciable decrease in emission intensities was observed upon the addition of the complexes to EB-CT-DNA system (**Fig. 4**), which is due to the intercalation of the complexes to DNA base pairs replacing some EB molecules from the EB-CT-DNA system, or the groove binding of the complexes to DNA leading to the energy/electron transfer from the guanine base of DNA to the MLCT of the complexes.<sup>42,43</sup> Although these results do not rule out the intercalating binding mode of the ligands in between the base pairs displacing EB from binding sites, because of the forming of the extensive hydrogen-bond for the ligands one can expect the groove binding of the complexes to DNA.

The quenching efficiency was evaluated by the Stern–Volmer constant  $K_{sq}$  which was determined using the classical Stern–Volmer equation:<sup>44</sup>

$$I_0/I = 1 + K_{sq} r \quad (2)$$

where  $I_0$  and  $I$  represent the fluorescence intensities in the absence and presence of complexes, respectively, and  $r$  corresponds to the concentration ratio of the complexes to DNA.  $K_{sq}$  is a linear Stern-Volmer quenching constant and is obtained from the linear regression of  $I_0/I$  with  $r$ . The  $K_{sq}$  values were found to be 0.167 and 0.072 for **1** and **2**, respectively, following the order of **1** > **2**. The apparent binding constant ( $K_{app}$ ) was calculated using the equation  $K_{EB} [EB] = K_{app} [Complex]$ , where  $[EB] = 8.0 \mu\text{M}$ ,  $K_{EB} = 1.0 \times 10^7 \text{ M}^{-1}$ ,<sup>45</sup> and the complex concentration was the value at 50% reduction of the fluorescence intensity of EB obtained from the linear regression of  $I/I_0$  with  $[Complex]$  (**Fig. 4c**). The  $K_{app}$  values were calculated to be  $9.82 \times 10^5 \text{ M}^{-1}$  for **1**,  $7.35 \times 10^5 \text{ M}^{-1}$  for **2**, respectively. These facts suggest that **1** has stronger binding affinity for CT-DNA as compared to **2**, which is in accord with the above absorption titrations data.

**Fig. 4**

**CD spectral studies.** CD spectroscopy is a useful technique in monitoring the morphology variations of DNA during small molecules-DNA interactions. The CD spectrum of CT-DNA exhibits a positive band at 275 nm due to base stacking and a negative band at 245 nm due to right-handed helicity of B-DNA. As increasing the concentration of the complexes, the intensities of both the negative and positive bands of CT-DNA decreased (shifting to zero levels) (**Fig. 5**), which is a clear indication of the interactions between the complexes and CT-DNA. The decreased intensity in the negative band suggests the complexes can unwind the DNA helix and reduce its stability to a certain extent.<sup>46</sup> Moreover, prominent red shift for both negative bands (**1**, 246 → 250 nm; **2**, 246 → 248 nm) and positive bands (**1**, 275 → 284 nm; **2**, 276 → 281 nm) were observed, indicating that the binding disturbed the right-handed helicity and base stacking of DNA, thus induced certain conformational changes of the secondary structure within the DNA molecule, such as the conversion from a more B-like to a more C-like structure.<sup>47</sup> These changes are indicative of a non-intercalative DNA-binding mode of the complexes, probably a groove binding nature. Furthermore, the changing intensity follows the tendency of **1** > **2**, in line with the results obtained by UV and fluorescence spectroscopy.

**Fig. 5**

**Viscometric determination.** In the absence of crystallographic structural data or NMR spectra, viscosity of DNA that is sensitive to length changes is regarded as the least ambiguous and the most critical clues of a DNA binding mode in

solution.<sup>48</sup> In general, intercalating agents are expected to elongate the double helix to accommodate the ligands in between the base pairs leading to an increase in the viscosity of DNA. In contrast, complex that binds exclusively in the DNA grooves by partial and/or non-classical intercalation typically cause less pronounced (positive or negative) or nochange in DNA solution viscosity.<sup>49,50</sup> The relative viscosities of CT-DNA in the presence of the complexes and ethidium bromide (an intercalator) are shown in **Fig. 6**. Upon continuous addition of the complexes, relatively inapparent decrease in DNA viscosity was observed. However, when the concentration of ethidium bromide was increased, there was a substantial increase in DNA viscosity. These changes in DNA viscosity ruled out the intercalative binding mode of the complexes to DNA, and is consistent with DNA groove binding suggested above.<sup>36,51</sup> The decreased degree of viscosity associated with the affinity of the complexes to DNA follows the order of **1 > 2**, which is in accord with our foregoing hypothesis.

**Fig. 6**

### DNA Cleavage properties

**DNA cleavage in the absence and presence of ascorbate.** To evaluate the chemical nuclease activity of the complexes, the pBR322 plasmid DNA as a substrate was incubated with the complexes and the cleavage reactions on plasmid DNA were monitored by agarose gel electrophoresis (**Fig. 7**). No significant DNA cleavage was observed for the free complexes (no ascorbate) (lane 5), While in the presence of ascorbate (0.5 mM), the concentration dependent relaxation of supercoiled circular (Form I) of pBR322 DNA into nicked circular (Form II), even linear (Form III) was achieved for both the complexes (lanes 6–9). Under comparable experimental conditions, DNA-nicking efficiencies of the complexes follow the trend **1 > 2**, which can be due to the fact that binding of the complexes to plasmid DNA can loosen the SC DNA (Form I), thus the DNA cleavage efficiencies were related to the DNA binding affinity of the complexes. These results show that the nuclease efficiency of the complexes is dependent on the activation of ascorbate, thus the DNA cleavage induced by the complexes should be oxidative. To ensure that the copper(II) complexes was solely responsible for the cleavage, control experiments were performed (lanes 1–4) under identical experimental conditions. The results show that free  $\text{Cu}(\text{ClO}_4)_2$ , glygly and ligands (PyTA/PzTA) hardly exhibited any DNA cleavage activity even in the presence of ascorbate, indicating that the active compounds responsible for the DNA cleavage were the complexes.

**Fig. 7**

**Reactive oxygen species responsible for DNA cleavage.** In order to explore the preliminary mechanism of DNA cleavage by the complexes, further investigation was performed using different typical scavengers under the above experimental conditions (**Fig. 8**). It is clear that in the presence of hydroxyl radical scavengers [DMSO (lane 3), tert-butyl alcohol (lane 4), and ethanol (lane 5)], the cleavage was inhibited significantly, indicating the possibility of the involvement of the hydroxyl radical. The singlet oxygen quenchers [TMP (lane 6) and  $\text{NaN}_3$  (lane 7)] exhibited no obvious inhibition for the DNA cleavage, which rules out the involvement of singlet oxygen or singlet oxygen-like entities. Moreover, the DNA cleavage of the complexes was observably promoted in the presence of superoxide anion radical scavenger [SOD (lane 8)] with no distinct DNA cleavage for the free SOD (lane 1). This indicates that the superoxide radical anion was not directly involved in the DNA strand scission but involved in a round-about way. Based on the above results, the DNA cleavage of the complexes may involve in a redox pathway in which the Cu(II) compounds generate reactive Cu(I) species with the subsequent generation of hydroxyl radicals, similar to the one proposed by Sigman for the bis(phen)copper(II) complex.<sup>52</sup>

**Fig. 8****Superoxide dismutase activity**

Superoxide dismutase (SOD) is a ubiquitous enzyme with an essential role in antioxidant defense through catalysis of the disproportionation of  $\cdot\text{O}_2^-$  under physiological conditions. Recent evidences continue to accrue, implicating that  $\cdot\text{O}_2^-$  contributes to the pathogenesis of a number of human diseases, such as inflammatory damage,<sup>53</sup> membrane and DNA damage,<sup>54</sup> cancer and acquired immunodeficiency syndrome.<sup>55</sup> Therefore, further investigation of the SOD-like activities of the new DNA base analogs based copper(II)-dipeptide complexes to figure out the relation between  $\cdot\text{O}_2^-$  and human diseases especially types of cancer would give us another special purport or meaning in life sciences. The effects of the complexes on the NBT photoreduction and corresponding plots of percent inhibition with an increase in concentration of the complexes are presented in **Fig. 9**. Evidently, the complexes exhibit excellent SOD-like activity with  $\text{IC}_{50}$  values of 0.091 and 0.114  $\mu\text{M}$  for **1** and **2**, respectively, which could be related to the distorted square-pyramidal geometry of the complexes, with fast exchange of water molecules weakly linked to the

center copper(II), and the coordination site belonging to nitrogen heteroatomic rings such as pyridine and pyrazine important for a high SOD activity.<sup>27</sup> Though the activity of the complexes is about 2 – 3 times less than that of the native Cu, Zn-SOD ( $IC_{50} \sim 0.04 \mu\text{M}$ ),<sup>56</sup> the complexes are potent SOD mimics due to their much lower molecular weight compared with that of the native SOD enzyme (MW 32000 D).

### Fig. 9

#### In vitro cytotoxicity

The in vitro cytotoxic activities of the complexes against human carcinoma cell lines of HepG2 (hepatocellular), HeLa (cervical), A549 (pulmonary) and U87 (cerebral glioma) were assessed by MTT assay. The concentrations of the complexes ranged from 3.125  $\mu\text{M}$  to 200  $\mu\text{M}$ . The cytotoxicity of the complexes was found to be concentration-dependent, which is to say that the average cell viability ratio decreased with increasing concentrations of the tested compounds. The  $IC_{50}$  values of the complexes, cisplatin and 5-Fluorouracil by MTT assay after a 48 h treatment were shown in **Fig. 10**. Complex **1** exhibited higher in vitro cytotoxicity against the selected tumor cell lines except for HepG2 than 5-Fluorouracil, a widely used clinical antitumor drug, but relative lower cytotoxicity than cisplatin, and complex **2** showed certain cytotoxic activity, which is lower than 5-Fluorouracil and cisplatin. Thus, the in vitro cytotoxicity toward HepG2, HeLa, A549 and U87 cell lines for the complexes follows the order **1** > **2**, which coincides with the DNA-cleavage and SOD-like activities of the two complexes. This fact indicates that the antitumor activity for the complexes may be closely related to their DNA interaction and disproportionation of  $\cdot\text{O}_2^-$  accrued in tumour cell. Furthermore, the cytotoxicity toward the four tested carcinoma cell lines follows the trend: A549 > HeLa > HepG2 > U87. These observations indicate that complex **1** has the potential to act as an effective metallopeptide-based chemotherapeutic agents, especially targeting for A549 cell lines.

### Fig. 10

#### HSA binding properties

**Fluorescence enhancement of the complexes by HSA.** The effects of HSA on the emission spectra of the complexes are shown in **Fig. 11**. Upon addition of increasing amounts of HSA to the complexes, a prominent fluorescence enhancement with a blue-shift (374 nm  $\rightarrow$  368 nm) for both the complexes was observed, which ascribed

to a reduction in the polarity of the microenvironment around the complexes resulting from the binding of the complexes to the hydrophobic cavity of protein. The protein binding decreased the freedom of the rotation or vibration for the complexes, which could be regarded as another reason for fluorescence enhancement of the complexes.<sup>57</sup>

### Fig. 11

**Fluorescence quenching of HSA by the complexes.** Fluorescence spectroscopy is a powerful method universally utilized to explore the interactions between small molecules and biomacromolecules. **Fig. 12** shows the effects of concentration of the complexes on the fluorescence emission of HSA. The fluorescence emission of the characteristic broad band at 344 nm of HSA quenched regularly with the increasing concentration of the complexes, which confirms some interactions between the complexes and HSA and alteration of the local microenvironment around the Trp-214 residue in HSA. No prominent red shift or hypsochromic shift was observed suggesting no conformational change of the tertiary structure of HSA.

### Fig. 12

The fluorescence quenching mechanism in the complex–HSA systems can be deduced from the fluorescence quenching data at different temperatures (300 and 310 K) using the classical Stern–Volmer equation:<sup>58</sup>

$$\frac{F_0}{F} = 1 + K_{SV}[Q] = 1 + k_q\tau_0[Q] \quad (3)$$

where  $F_0$  and  $F$  represent the fluorescence intensity in the absence and presence of quencher, respectively.  $K_{SV}$ ,  $k_q$ ,  $\tau_0$  and  $[Q]$  are the Stern–Volmer quenching constant, the quenching rate constant of biomolecule, the average lifetime of biomolecule without quencher ( $k_q = 10^8$  s) and the concentration of quencher, respectively. The  $K_{SV}$  and  $k_q$  values were calculated from the Stern–Volmer quenching plots of  $F_0/F$  versus  $[Q]$  at two different temperatures and summarized in **Table 3**. The obtained results revealed that the  $K_{SV}$  values inversely correlated with temperature, and the  $k_q$  values ( $10^{12} - 10^{13} \text{ M}^{-1} \text{ s}^{-1}$ ) are much higher than the limiting diffusion constant  $K_{dif}$  of biomolecule ( $K_{dif} = 2.0 \times 10^{10} \text{ M}^{-1} \text{ s}^{-1}$ ),<sup>59</sup> manifesting that the fluorescence quenching was likely to occur via a static quenching mechanism involving a specific interaction between HSA and the complexes.<sup>30</sup>

**Table 3** Quenching, binding and thermodynamic parameters of the complexes-HSA interactions at different temperatures<sup>a</sup>

	<i>T</i> (K)	$10^{-13} k_q$ ( $M^{-1} s^{-1}$ )	$10^{-5} K_{sv}$ ( $M^{-1}$ )	<i>R</i>	$10^{-6} K_a$ ( $M^{-1}$ )	<i>n</i>	<i>R</i>	$\Delta H$ (KJ mol <sup>-1</sup> )	$\Delta G$ (KJ mol <sup>-1</sup> )	$\Delta S$ (KJ mol <sup>-1</sup> K <sup>-1</sup> )
HSA- 1	300	1.0543	1.0543	0.9843	3.85	1.34	0.9986		-37.82	0.08
	310	0.9311	0.9311	0.9860	3.24	1.34	0.9984	-13.34	-38.64	
HSA-2	300	0.5847	0.5847	0.9955	0.26	1.14	0.9987		-31.10	0.44
	310	0.5443	0.5443	0.9951	0.96	1.27	0.9999	100.99	-35.50	

<sup>a</sup>*R* is the linear correlated coefficient.

**Binding parameters.** For a static quenching, the binding constant ( $K_a$ ) and the number of binding sites ( $n$ ) can be determined using the following Scatchard equation:<sup>57</sup>

$$\log[(F_0 - F)/F] = \log K_a + n \log[Q] \quad (4)$$

The  $K_a$  and  $n$  values obtained from the intercepts and slopes, respectively, of the corresponding linear fitting plots of  $\log[(F_0 - F)/F]$  versus  $\log[Q]$  (**Fig. 13**) are summarized in **Table 3**. The values of  $n$  and  $K_a$  suggest that the complexes bound to HSA according to the molar ratio of 1:1, and **1** exhibited higher HSA binding affinity than that of **2**. Besides, the  $n$  values are basically positive correlation with the  $K_a$  values, which implies a direct relation between the binding constant and the number of binding sites.

**Fig. 13**

**Thermodynamic parameters and binding mode.** Generally, small molecules bind to biomacromolecules through weak interactions mainly including hydrogen bonds, van der Waals forces, electrostatic and hydrophobic interactions. The binding mode can be determined by the thermodynamic parameters, enthalpy change ( $\Delta H$ ), entropy change ( $\Delta S$ ) and free energy change ( $\Delta G$ ). From the thermodynamic standpoint,  $\Delta H > 0$  and  $\Delta S > 0$  suggest a hydrophobic interaction,  $\Delta H < 0$  and  $\Delta S < 0$  indicate the formation of van der Waals force or hydrogen bond, and  $\Delta H \approx 0$  and  $\Delta S > 0$  reflect an electrostatic force.<sup>60</sup> 300 and 310 K were chosen for the thermodynamic measurements, and the thermodynamic parameters can be calculated from the Van't Hoff equation:

$$\ln \frac{K_2}{K_1} = -\frac{\Delta H}{R} \left( \frac{1}{T_2} - \frac{1}{T_1} \right) \quad (5)$$

$$\Delta G = \Delta H - T\Delta S = -RT \ln K \quad (6)$$

where  $K_1$  and  $K_2$  are the binding constants at temperatures  $T_1$  and  $T_2$ , respectively,  $K$  is the equilibrium binding constant, which is analogous to the effective quenching constants  $K_a$ , and  $R$  is the gas constant. The calculated thermodynamic parameters were listed in **Table 3**. The negative values of  $\Delta G$  for both complexes reveal that the protein binding process is spontaneous, and the lower  $\Delta G$  values for **1** indicate its higher binding affinity. The negative  $\Delta H$  and positive  $\Delta S$  values for **1** suggest that hydrophobic interaction played a major role in the **1**-HSA interaction and contributed to the stability of **1**, and hydrogen bonding were also involved, which was further confirmed by the molecular docking studies. In addition, the both positive  $\Delta H$  and  $\Delta S$  values make clear that the hydrophobic interaction was the main driving force in **2**-HSA binding process.

### Conformation investigations

**UV spectroscopy.** To explore the structural changes of protein induced by the complexes, the UV absorption spectra of HSA with various amounts of the complexes were measured. **Fig. 14** shows a strong absorption peak at 220 nm attributed to the  $n \rightarrow \pi^*$  transition for the peptide bond of  $\alpha$ -helix, and a weak absorption peak at 280 nm due to the  $\pi \rightarrow \pi^*$  transition for the phenyl rings in aromatic acid residues (Trp, Tyr and Phe).<sup>61</sup> As the increase in the amounts of the complexes, a remarkable decrease in the absorption intensity at 220 nm and significant red shifts (8 - 9 nm) were observed, which can be attributed to the perturbation of  $\alpha$ -helix induced by a specific interaction between the complexes and protein. Simultaneously, the intensity of the absorption peak at 280 nm was decreased by titration of the complexes, which may be due to the fact that aromatic acid residues originally buried in a hydrophobic cavity were exposed to an aqueous milieu to a certain degree. Besides, the  $\pi$ - $\pi$  stacking interaction between the aromatic rings of the complexes and the phenyl rings of aromatic acid residues could be another reason for the hypochromism. These changes of absorption spectra make a clear indication that the microenvironment around the three aromatic acid residues was altered induced by the binding of the complexes, and the secondary structure of HSA was changed to some extent.

**Fig. 14**

**CD spectroscopy.** CD measurement was performed in the presence of the complexes at different concentrations to monitor the conformation changes of protein. As shown in **Fig. 15**, two negative bands at 208 and 222 nm attributed to  $\pi \rightarrow \pi^*$  and  $n \rightarrow \pi^*$  transfers, respectively, are observed in the CD spectrum of free HSA (line a), characteristic of  $\alpha$ -helical proteins.<sup>61</sup> The ellipticity of HSA decreased moderately with the increase in concentration of the complexes (lines b, c and d), implying some loss (**1**, 65.5%  $\rightarrow$  54.9%; **2**, 68.0%  $\rightarrow$  57.7%) of the  $\alpha$ -helical secondary structure. This may reveal that the complexes bound to the amino acid residues of main polypeptide chain of HSA and destroyed their hydrogen bonding networks, concomitantly the protein's secondary structure. Besides, the loss of  $\alpha$ -helical content also indicates that the binding induced a little unfolding of the polypeptides of HSA, which led to the increase in the exposure of some hydrophobic regions previously buried. However, the CD spectra before and after addition of the complexes are similar in shape, suggesting a predominant  $\alpha$ -helical conformation of HSA in this system.

**Fig. 15**

**Synchronous FL spectroscopy.** Synchronous fluorescence spectroscopy can provide valuable information on the microenvironment near different fluorophores, thus identified as an effective method in monitoring the microenvironment changes of proteins. When the scanning interval between excitation and emission wavelength ( $\Delta\lambda$ ) is stabilized at 15 and 60 nm, the spectra can provide the specific microenvironment information of tyrosine and tryptophan residues, respectively. The shift in the position of the maximum emission wavelength corresponds to changes of the polarity around the fluorophore of amino acid residues.<sup>62</sup> **Fig. 16** shows the synchronous fluorescence spectra of HSA with various amounts of the complexes. The fluorescence intensity at  $\Delta\lambda = 60$  nm decreased steadily while the fluorescence intensity at  $\Delta\lambda = 15$  nm increased slightly, which indicates that the protein binding mainly occurred in the position of the tryptophan residue. No prominent red or hypsochromic shifts at  $\Delta\lambda = 15$  nm and 60 nm were observed, suggesting that the microenvironment around the tryptophan and tyrosine residues did not undergo obvious changes during the binding process.

**Fig. 16**

**3D fluorescence spectroscopy.** To provide profound insight into the conformational changes of protein induced by the complexes, 3D fluorescence spectroscopy were performed on HSA and complex-HSA system. The 3D fluorescence spectra and corresponding contour maps of HSA and complex–HSA system are shown in **Fig. 17**, and the obtained characteristic parameters are listed in **Table 4**. Peak a and peak c are the Rayleigh scattering peak ( $\lambda_{\text{ex}} = \lambda_{\text{em}}$ ) and the second-ordered scattering peak ( $\lambda_{\text{em}} = 2\lambda_{\text{ex}}$ ), respectively. Peak b (280, 346 nm,  $\lambda_{\text{ex}}, \lambda_{\text{em}}$ ) reflected the spectral behaviors of the tryptophan and tyrosine residues, and its location and intensity are closely related to the microenvironmental polarity around these residues.<sup>63</sup> As Fig. 17 shows, The fluorescence intensity of peaks a and b decreased significantly to a different extent in the presence of the complexes, and their maximum emission wavelength was also changed. The decrease in peak a demonstrates that the structure of the peptide strands has changed in the presence of the complexes, which agrees with the decrease of  $\alpha$ -helix in the CD spectra. The decrease in peak b reveals that the binding of the complexes to HSA induced special conformational changes of HSA, which are related to the hydrophobic microenvironment near the tryptophan and tyrosine residues. From above results, it can be deduced that HSA experienced a slight unfolding of the polypeptides in the presence of the complexes, corroborated well the results obtained from UV, synchronous FL and CD.

**Fig. 17**

**Table 4** 3D fluorescence spectral characteristic parameters of HSA in the absence and presence of **1** or **2**

HSA				HSA-1 / HSA-2 system			
Peak position	$\lambda_{\text{ex}}/\lambda_{\text{em}}$ (nm/nm)	$\Delta\lambda$	Intensity	Peak position	$\lambda_{\text{ex}}/\lambda_{\text{em}}$ (nm/nm)	$\Delta\lambda$	Intensity
Peak a	280/280–360/360	0	105.7-227.2	Peak a	280/280–360/360	0	67.51-185.8 / 66.12-188.9
Peak b	280/340	60	347.2	Peak b	280/340	60	194.7 / 262.9

### Molecular docking studies

**Molecular docking with DNA.** Molecular docking is a particularly powerful technique for understanding the drug–DNA interaction in the rational drug design, as well as in the mechanistic study by placing a small molecule into the binding site of the DNA target specific region mainly in a non-covalent fashion.<sup>64</sup> Targeting the DNA minor groove for a small molecule has long been regarded as an important pattern in molecular recognition of a specific DNA sequence.<sup>65</sup> An energetically favorable docked pose obtained from the rigid molecular docking of **1** with a DNA duplex

of sequence d(CGCGAATTCGCG)<sub>2</sub> dodecamer (PDB ID : 1BNA) is shown in **Fig. 18**. Obviously, complex **1** fits snugly into the curved contour of the DNA target in the minor groove and is situated within an A–T rich region, which brings about van der Waals and hydrophobic interactions with DNA functional groups that define the groove. Moreover, the plane forming between the PyTA and copper(II) arranged in a parallel fashion with respect to the deoxyribose groove walls of DNA and was stabilized by extensive hydrogen bonds mainly induced by –NH<sub>2</sub> of PyTA, viz. Complex:H5A...1BNA: B:DA-17:N3 (1.983 Å), Complex:H5A...1BNA:B:DA-18:O4' (1.969 Å), Complex:H5B...1BNA:A:DC-9:O2 (2.104 Å), Complex:H6A...1BNA:A:DT-8:O2 (1.958Å) and Complex: O3...1BNA:B:DG-16:H22 (2.094 Å), while the remaining pyridine group points outside the minor groove. The resulting relative binding energy of docked **1** with DNA was found to be –38.35 kJ mol<sup>-1</sup>, which is consistent with the moderate binding constant obtained from absorption spectroscopic titration. Thus, the molecular modeling technique has made a convictive complement to the spectroscopic methods, which further confirms an outside DNA groove binding mode for **1** with a moderate binding affinity.

**Fig. 18**

**Molecular docking with HSA.** In order to further rationalize the observed protein-binding assays of the complexes, molecular docking studies were performed to explore the exact binding sites and affinity inside the molecular target HSA. Descriptions of the 3D structure of crystalline albumin have revealed that HSA comprises three homologous domains (denoted I, II, and III): I (residues 1–195), II (196–383) and III (384–585), each domain has two subdomains (A and B) that assemble to form heart shaped molecule. The principal region of drug binding sites of HSA are located in hydrophobic cavities in subdomains IIA and IIIA, corresponding to sites I and II, respectively, and tryptophan residue (Trp-214) of HSA in subdomain IIA.<sup>66</sup> The resulting docked pattern with the lowest binding free energy is presented in **Fig. 19a**. Complex **1** is located in hydrophobic cavities in subdomains IIA and IIIA, but mainly in IIA, suggesting the existence of hydrophobic interaction between **1** and HSA. Complex **1** partly enters the hydrophobic cavity of subdomain IIA, resulting in the fluorescence quenching of Trp-214, which forcefully explains the efficient fluorescence quenching of HSA emission in the presence of **1**. Furthermore, the formation of extensive hydrogen bonds (**Fig. 19b**), including Complex:H5A...1H9Z:A:ASP451:OD1 (2.075Å), Complex:H6A...1H9Z:A:LYS195:O (1.798Å), Complex: O1W...1H9Z:A:ARG218:HH22 (1.631Å), Complex:O3...1H9Z:A:ARG222: HH21 (1.727 Å), decreased the

hydrophilicity while increased the hydrophobicity, which play an important role in stabilizing the complex **1**-HSA system. The simulation results coincide well with the above thermodynamic analysis and fluorescence quenching mechanism. Hence, we can conclude that there is a mutual complement between spectroscopic techniques and molecular modeling.

### Fig. 19

## Conclusions

In this paper, we have designed and synthesized two water-soluble DAT derivatives based copper(II)-dipeptide complexes with one dimensional chain structures. The effects of the complexes on the binding propensity of DNA and HSA were examined to elucidate the mechanism and mode of action at the molecular targets. Selectively binding to the DNA minor groove has been confirmed by using various physico-chemical and molecular docking techniques. The complexes exhibit prominent DNA cleavage in the presence of ascorbate via an oxidative mechanism induced by  $\cdot\text{OH}$  and  $\cdot\text{O}_2^-$ , besides prominent SOD-like activity. Notably, the complexes possess considerable cytotoxicity toward HepG2, HeLa, A549 and U87 cell lines, following the order **1** > **2**. Additionally, multispectroscopic evidence indicates the complexes bind to HSA mainly via hydrophobic interaction in subdomain IIA with moderate affinity, validated by molecular docking studies. These findings make a clear indication that DAT derivatives based copper(II)-dipeptide complexes, as DNA minor groove binders, have the potential to be nucleic acid molecular probes and new effective metallopeptide-based chemotherapeutic agents.

## Acknowledgments

We are grateful to the 211 Engineering Key Project (2009B010100001) of South China Agricultural University for generous financial support.

## Appendix A. Supplementary data

Detailed crystallographic data for the crystal structural analysis have been deposited with the Cambridge Crystallographic Data Centre, CCDC No. 977247. Copies of this information may be obtained free of charge from The Director, CCDC, 12 Union Road, Cambridge CB2 1EZ, UK (fax: +44-1223-336033; e-mail: deposit@ccdc.cam.ac.uk or <http://www.ccdc.cam.ac.uk>).

## Notes and references

- 1 B. Rosenberg, L. VanCamp, J. E. Trosko and V. H. Mansour, *Nature*, 1969, **222**, 385.
- 2 Y. Xie, G. G. Miller, S. A. Cubitt, K. J. Soderlind, M. J. Allalunis-Turner and J. W. Lown, *Anticancer Drug Res.*, 1997, **12**, 169.
- 3 R. Gust, W. Beckb, G. Jaouenc and H. Schenberger, *Coord. Chem. Rev.*, 2009, **253**, 2742.
- 4 P. J. Dyson, M. J. Rose, N. L. Fry, R. Marlow, L. Hinck and P. K. Mascharak, *J. Am. Chem. Soc.*, 2008, **130**, 8834.
- 5 P. J. Bednarski, F. S. Mackay and P. J. Sadler, *Anticancer Agents Med. Chem.*, 2007, **7**, 75.
- 6 S. Tabassum, W. M. Al-Asbahy, M. Afzal, F. Arjmanda and V. Bagchib, *Dalton Trans.*, 2012, **41**, 4955.
- 7 C. Y. Gao, X. Qiao, Z. Y. Ma, Z. G. Wang, J. Lu, J. L. Tian, J. Y. Xu and S. P. Yan, *Dalton Trans.*, 2012, **41**, 12220.
- 8 S. Tabassum, W. M. Al-Asbahy, M. Afzal and F. Arjmand, *J. Photochem. Photobio. B*, 2012, **114**, 132.
- 9 B. N. Ames, M. K. Shigenaga and T. M. Hagen, *Proc. Natl. Acad. Sci. USA*, 1993, **90**, 7915.
- 10 a) P. G. A. Janssen, S. Jabbari-Farouji, M. Surin, X. Vila, J. C. Gielen, T. F. A. de Greef, M. R. J. Vos, P. H. H. Bomans, N. A. J. M. Sommerdijk, P. C. M. Christianen, P. Leclere, R. Lazzaroni, P. van der Schoot, E. W. Meijer and A. P. H. J. Schenning, *J. Am. Chem. Soc.*, 2009, **131**, 1222. b) P. G. A. Janssen, J. Vandenberg, J. L. J. Van Dongen, E. W. Meijer and A. P. H. J. Schenning, *J. Am. Chem. Soc.*, 2007, **129**, 6078.
- 11 K. Srinivas, U. Srinivas, K. Bhanuprakash, K. Harakishore, U. S. N. Murthy, V. J. Rao, *Eur. J. Med. Chem.*, 2006, **41**, 1240.
- 12 B. Klenke, M. Stewart, M. P. Barrett, R. Brun, I. H. Gilbert, *J. Med. Chem.*, 2001, **44**, 3440.
- 13 S. Nozaki, M. Maeda, H. Tsuda, G. W. Sledge, *Breast Cancer Research and Treatment*, 2004, **83**, 195.
- 14 D. W. Ludovici, R. W. Kavash, M. J. Kukla, C. Y. Ho, H. Ye, B. L. De Corte, K. Andries, M.-P. de Bethune, H. Azijn, R. Pauwels, H. E. L. Moereels, J. Heeres, L. M. H. Koymans, M. R. de Jonge, K. J. A. Van Aken, F. F. D. Daeyaert, P. J. Lewi, K. Das, E. Arnold and P. A. J. Janssen, *Bioorg. Med. Chem. Lett.*, 2001, **11**, 2229.
- 15 R. J. Mattson, D. J. Denhart, J. D. Catt, M. F. Dee, J. A. Deskus, J. L. Ditta, J. Epperson, H. D. King, A. Gao, M. A. Poss, A. Purandare, D. Tortolani, Y. F. Zhao, H. Yang, S. Yeola, J. Palmer, J. Torrente, A. Stark and G. Johnson, *Bioorg. Med. Chem. Lett.*, 2004, **14**, 4245.
- 16 B. L. Mylari, P. J. Oates, W. J. Zembrowski, D. A. Beebe, E. L. Conn, J. B. Coutcher, M. T. O'Gorman, M. C. Linhares and G. J. Withbroe, *J. Med. Chem.*, 2002, **45**, 4398.
- 17 B. R. Henke, T. G. Consler, N. Go, R. L. Hale, D. R. Hohman, S. A. Jones, A. T. Lu, L. B. Moore, J. T. Moore, L. A. Orband-Miller, R. G. Robinett, J. Shearin, P. K. Spearing, E. L. Stewart, P. S. Turnbull, S. L. Weaver, S. P. Williams, G. B. Wisely, M. H. Lambert, *J. Med. Chem.*, 2002, **45**, 5492.
- 18 a) F. Saczewski and A. Bulakowska, *Eur. J. Med. Chem.*, 2006, **41**, 611. b) F. Saczewski, A. Bulakowska, P. Bednarski and R. Grunert, *Eur. J. Med. Chem.*, 2006, **41**, 219.
- 19 P. Uma Maheswari and M. Palaniandavar, *J. Inorg. Biochem.*, 2004, **98**, 219.
- 20 D. E. Wemmer, *Biopolymers*, 1999, **52**, 197.

- 21 P. G. Baraldi, A. Bovero, F. Fruttarolo, D. Preti, M. A. Tabrizi, M. G. Pavani and R. Romagnoli, *Med. Res. Rev.*, 2004, **24**, 475.
- 22 a) A. Duong, T. Maris and J. D. Wuest, *Inorg. Chem.*, 2011, **50**, 5605. b) A. Duong, V. Metivaud, T. Maris and J. D. Wuest, *Crystal Growth and Design*, 2011, **11**, 2026
- 23 D. L. Ma, C. M. Che, F. M. Siu, M. S. Yang and K. Y. Wong, *Inorg. Chem.*, 2007, **46**, 740.
- 24 P. R. Reddy and P. Manjula, *Chem. Bio.*, 2007, **4**, 468.
- 25 F. H. Case and E. Koft, *J. Am. Chem. Soc.*, 1959, **81**, 90.
- 26 a) G. M. Sheldrick, *SHELXS-97, Program for the Solution of Crystal Structure*, University of Gottingen, Germany, 1997. b) G. M. Sheldrick, *SHELXL-97, Program for the Refinement of Crystal Structure*, University of Gottingen, Germany, 1997.
- 27 X. Y. Le, S. R. Liao, X. P. Liu and X. L. Feng, *J. Coord. Chem.*, 2006, **59**, 985.
- 28 T. Mosmann, *J. Inorg. Biochem.*, 1983, **65**, 55.
- 29 C. G. Ricci, P. A. Netz, *J. Chem. Inf. Model.*, 2009, **49**, 1925.
- 30 S. Tabassum, W. M. Al-Asbahy, M. Afzal, F. Arjmand and R. H. Khan, *Mol. BioSyst.*, 2012, **8**, 2424.
- 31 W. J. Geary, *Coord. Chem. Rev.*, 1971, **7**, 81.
- 32 W. L. Liu, Y. Zou, C. L. Ni, Z. P. Ni, Y. Z. Li, Y. G. Yao and Q. J. Meng, *J. Coord. Chem.*, 2004, **57**, 899.
- 33 K. Nakamoto, *Infrared and Raman Spectra of Inorganic and Coordination Compounds (Part B)*, 6th Ed., John Wiley and Sons, New York, 2009, **58**, p. 65.
- 34 P. S. Subramanian, E. Suresh, P. Dastidar, S. Waghmode and D. Srinivas, *Inorg. Chem.*, 2001, **40**, 4291.
- 35 Z. A. Siddiqi, P. K. Sharma, M. Shahid and M. Khalid, *J. Photochem. Photobio. B*, 2013, **125**, 171.
- 36 Z. H. Xu, F. J. Chen, P. X. Xi, X. H. Liu and Z. Z. Zeng, *J. Photochem. Photobio. A*, 2008, **196**, 77.
- 37 E. C. Long and J. K. Barton, *Acc. Chem. Res.*, 1990, **23**, 271.
- 38 H. L. Chan, H. C. Liu, B. L. C. Tzeng, Y. S. Y. You, S. M. Peng, M. S. Yang and C. M. Che, *Inorg. Chem.*, 2002, **41**, 3161.
- 39 A. Wolfe, G. H. Shimer and T. Meehan, *Biochemistry*, 1987, **26**, 6392.
- 40 J. Olmsted and D. R. Kearns, *Biochemistry*, 1977, **16**, 3647.
- 41 B. C. Baguley and M. L. Bret, *Biochemistry*, 1984, **23**, 937.
- 42 M. Chauhan, K. Banerjee and F. Arjmand, *Inorg. Chem.*, 2007, **46**, 3072.
- 43 R. Indumathy, S. Radhika, M. Kanthimathi, T. Weyhermuller and B. U. Nair, *J. Inorg. Biochem.*, 2007, **101**, 434.
- 44 J. R. Lakowicz and G. Webber, *Biochemistry*, 1973, **12**, 4161.
- 45 K. D. Karlin, I. Cohenn, J. C. Hayes, A. Farooq and J. Zubieta, *Inorg. Chem.*, 1987, **26**, 147.
- 46 K. Karidi, A. Garoufis, N. Hadjiliadis and J. Reedijk, *Dalton Trans.*, 2005, 728.
- 47 S. Mahadevan and M. Palaniandavar, *Inorg. Chem.*, 1998, **37**, 693.
- 48 S. Satyanarayana, J. C. Dabrowiak and J. B. Chaires, *Biochemistry*, 1993, **32**, 2573.
- 49 J. M. Kelly, A. B. Tossi, D.J. McConnell and C. OhUigin, *Nucleic Acids Res.*, 1985, **13**, 6017.
- 50 D. Suh and J. B. Chaires, *Bioorg. Med. Chem.*, 1995, **3**, 723.

- 51 D. L. Ma, C. M. Che, F. M. Siu, M. Yang and K. Y. Wong, *Inorg. Chem.*, 2007, **46**, 740.
- 52 D. S. Sigman, *Biochemistry* 1990, **29**, 9097.
- 53 S. Cuzzocrea, D. P. Riley, A. P. Caputi and D. Salvemini, *Pharmacol. Rev.*, **2001**, 53, 135.
- 54 T. C. Pederson and S. D. Aust, *Biochem. Biophys. Res. Commun.*, 1973, **52**, 1071.
- 55 J. S. Valentine and P. J. Hart, *Proc. Natl. Acad. Sci. U.S.A.*, 2003, **100**, 3617.
- 56 H. Fu, Y. H. Zhou, W. L. Chen, Z. G. Deqing, M. L. Tong, L. N. Ji and Z. W. Mao, *J. Am. Chem. Soc.* 2006, **128**, 4924.
- 57 F. Samari, B. Hemmateenejad, M. Shamsipur, M. Rashidi and H. Samouei, *Inorg. Chem.*, 2012, **51**, 3454.
- 58 J. R. Lakowicz, *Principles of Fluorescence Spectroscopy*, 3rd ed., Springer, New York, 2006.
- 59 M.R. Eftink, *Fluorescence Quenching Reaction: Probing Biological Macromolecular Structures*, Biophysical and Biochemical Aspects of Fluorescence Spectroscopy, Plenum Press, New York, 1991.
- 60 P. D. Ross and S. Subramanian, *Biochemistry*, 1981, **20**, 3096.
- 61 Y. Q. Wang, X. Y. Wang, J. Wang, Y. M. Zhao, W. J. He and Z. J. Guo, *Inorg. Chem.*, 2011, **50**, 12661.
- 62 C. H. Ng, W. S. Wang, K. V. Chong, Y. F. Win, K. E. Neo, H. B. Lee, S. L. San, R. N. Z. R. A. Rahmand and W. K. Leonge, *Dalton Trans.*, 2013, **42**, 10233.
- 63 Y. Z. Zhang, B. Zhou, Y. X. Liu, C. X. Zhou, X. L. Ding and Y. Liu, *J. Fluoresc.*, 2008, **18**, 109.
- 64 R. Rohs, I. Bloch, H. Sklenar and Z. Shakked, *Nucleic Acids Res.*, 2005, **33**, 7048.
- 65 L. F. Pineda De Castro and M. Zacharias, *J. Mol. Recognit.*, 2002, **15**, 209.
- 66 D. C. Carter, X. M. He, S. H. Munson, P. D. Twigg, K. M. Gernert, M. B. Broom and T. Y. Miller, *Science*, 1989, **244**, 1195.

## Figure captions

**Fig. 1.** ORTEP view of the molecular structure for **1**, [Cu(glygly)(PyTA)]ClO<sub>4</sub>·1.5H<sub>2</sub>O. Negative ions and dissociative small molecules are omitted for clarity.

**Fig. 2.** The intra- and intermolecular weak interaction in [Cu(glygly)(PyTA)]ClO<sub>4</sub>·1.5H<sub>2</sub>O. (a) The ring-ring ( $\pi$ - $\pi$ ) stacking interactions; (b) the hydrogen-bond interactions.

**Fig.3.** Absorption spectra of **1** (a) and **2** (b) (50  $\mu$ M) in the absence and presence of increasing amounts of CT-DNA. The arrow ( $\downarrow$ ) shows the absorbance changes upon increasing the DNA concentration. Inset: linear plot for the intrinsic DNA binding constant ( $K_b$ ).

**Fig. 4.** Effect of the addition of **1** (a) and **2** (b) on the emission intensity of EB (8  $\mu$ M) bound to CT-DNA (10  $\mu$ M) in 5 mM Tris-HCl/50 mM NaCl buffer (pH 7.2) at room temperature. Inset: Stern–Volmer quenching curve.

**Fig. 5.** CD spectra of CT-DNA (100  $\mu$ M) in the absence and presence of **1** (a) and **2** (b) in Tris–HCl buffer at 25 °C.  $r=[\text{Complex}]/[\text{DNA}] = 0, 0.2, 0.4, 0.6, 0.8, 1.0$ .

**Fig. 6.** Effect of increasing amounts of the complexes and ethidium bromide on the relative viscosity of CT-DNA (200  $\mu$ M) in Tris–HCl buffer at 29 ( $\pm 0.1$ ) °C.  $[\text{Complex}]/[\text{DNA}] = 0, 0.05, 0.10, 0.15, 0.20, 0.25, 0.30, 0.35$ .

**Fig. 7.** Agarose gel electrophoresis patterns for the cleavage of pBR322 DNA by **1** (a) and **2** (b) at 37 °C after 2 h of incubation. Lane 0, DNA control; lane 1, DNA + Vc (0.5 mM); lane 2, DNA + Vc (0.5 mM) + Cu(ClO<sub>4</sub>)<sub>2</sub>·6H<sub>2</sub>O (20  $\mu$ M); lane 3, DNA + Vc (0.5 mM) + ligand (20  $\mu$ M); lane 4, DNA + Vc (0.5 mM) + glygly (20  $\mu$ M); lane 5, DNA + **1** or **2** (20  $\mu$ M); lanes 6-9, DNA + Vc (0.5 mM) + **1** or **2** (5, 10, 15 and 20  $\mu$ M, respectively)

**Fig. 8.** Agarose gel electrophoresis patterns for the cleavage of pBR322 DNA by **1** (a) and **2** (b) in the presence of different typical reactive oxygen species scavengers at 37 °C after 2 h of incubation. Lane 0, DNA control; lane 1, DNA + Vc (0.5 mM) + SOD (15 units); lane 2, DNA + Vc (0.5 mM) + **1** or **2** (10  $\mu$ M); lanes 3-8, DNA + Vc (0.5 mM) + **1** or **2** (10  $\mu$ M) + [DMSO (0.2 M), tert-butyl alcohol (0.2 M), ethanol (0.2 M), TMP (0.2 M), NaN<sub>3</sub> (0.2 M) and SOD (15 units), respectively]

**Fig. 9.** Effects of **1** (a) and **2** (b) on the NBT photoreduction and corresponding plots (c) of percent inhibition versus the Cu(II) complexes concentration.

**Fig. 10.** The histogram of IC<sub>50</sub> values for the cytotoxicity of the complexes, cisplatin and 5-Fluorouracil.

**Fig. 11.** Effect of HSA on the emission spectra of **1** (a) and **2** (b). [**1** or **2**] = 5.0  $\mu\text{M}$ , and [HSA]/[**1** or **2**] = 0, 0.2, 0.4, 0.8, 1.0, 1.2, 1.4; pH 7.4 and  $\lambda_{\text{ex}}$  320 nm.

**Fig. 12.** Changes in the fluorescence spectra of HSA (10  $\mu\text{M}$ ) and corresponding Stern–Volmer plots at different temperatures after the titration of the complexes; [**1** or **2**] = 0 – 26.0  $\mu\text{M}$ , pH 7.4 and  $\lambda_{\text{ex}}$  280 nm.

**Fig. 13.** Logarithmic plot of the fluorescence quenching of HSA at different temperatures.

**Fig. 14.** UV spectra of HSA (10  $\mu\text{M}$ ) in the absence and presence of **1** or **2** (10  $\mu\text{M}$ ).

**Fig. 15.** CD spectra and corresponding histogram of ratio of different secondary structures of HSA (1.5  $\mu\text{M}$ ) in the absence and presence of **1** (a) and **2** (b) (0, 3.0, 6.0, and 9.0  $\mu\text{M}$ , respectively, from a to d). pH 7.4, at room temperature.

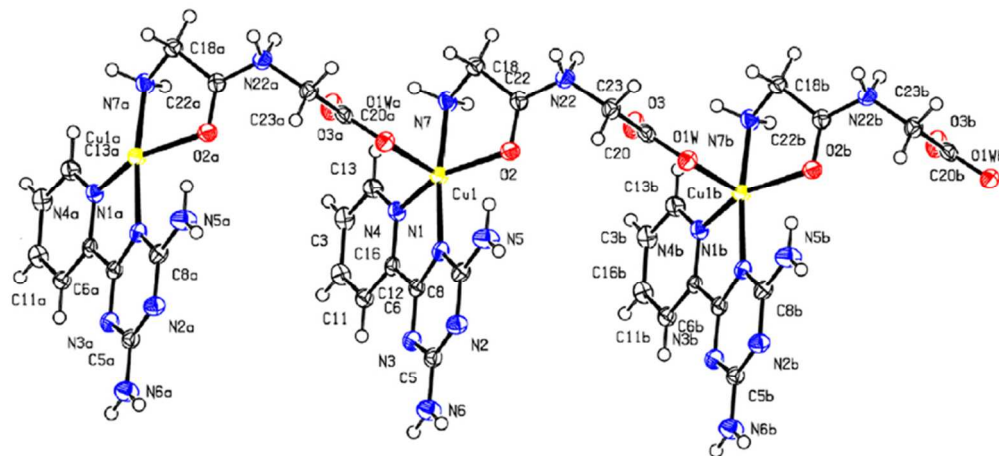
**Fig. 16.** Synchronous fluorescence spectra of HSA (10  $\mu\text{M}$ ) upon addition of **1** (a) and **2** (b) at  $\Delta\lambda = 15$  nm and  $\Delta\lambda = 60$  nm. [**1** or **2**] = 0 – 26.0  $\mu\text{M}$ .

**Fig. 17.** 3D fluorescence spectra and corresponding contour diagrams of HSA in the absence (a) and presence of **1** (b) or **2** (c); [HSA] = [**1** or **2**] = 10  $\mu\text{M}$ .

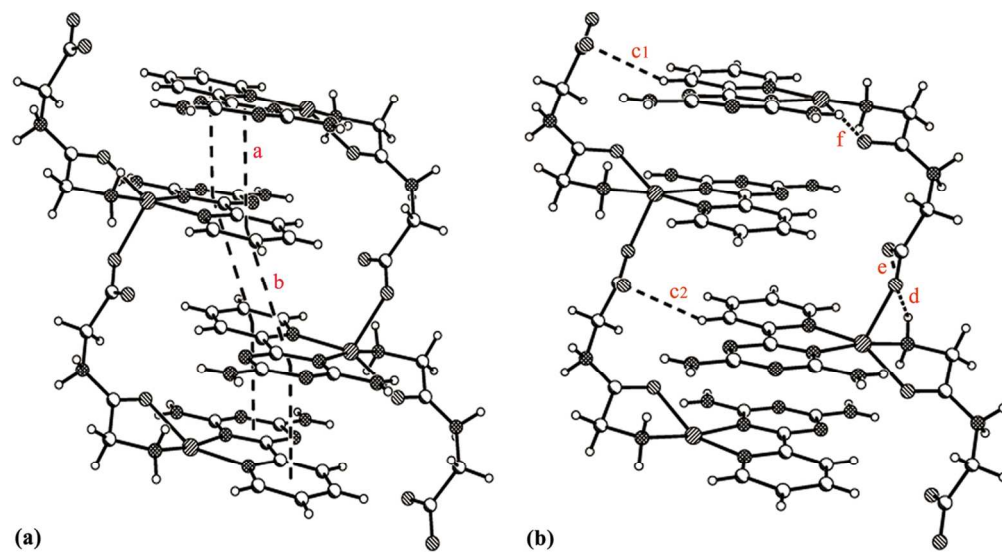
**Fig. 18.** A molecular docked model for **1** with a DNA dodecamer duplex of sequence d(CGCGAATTCGCG)<sub>2</sub> (PDB ID: 1BNA). (a) The full view of docking between **1** and 1BNA; (b) the binding mode between **1** and 1BNA represented in a cartoon form and the red dashed line showing hydrogen bond interactions between them.

**Fig. 19.** Docking of **1** in the active site of HSA (PDB ID: 1H9Z). (a) The full view of **1** in HSA with the complex and Trp-214 being depicted in space-filling representation; (b) the interaction mode between **1** and HSA represented in a cartoon form and the red dashed line showing hydrogen bond interactions between them.

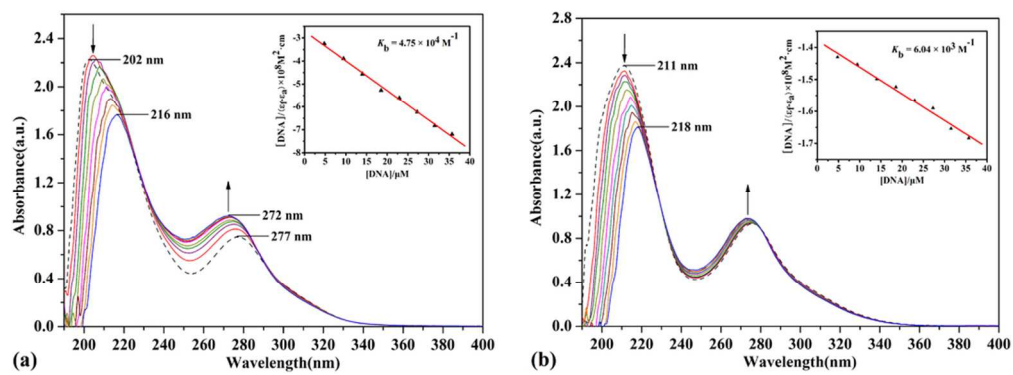




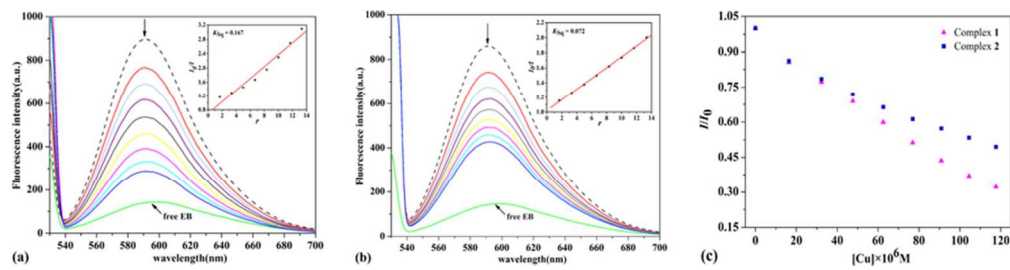
35x16mm (600 x 600 DPI)



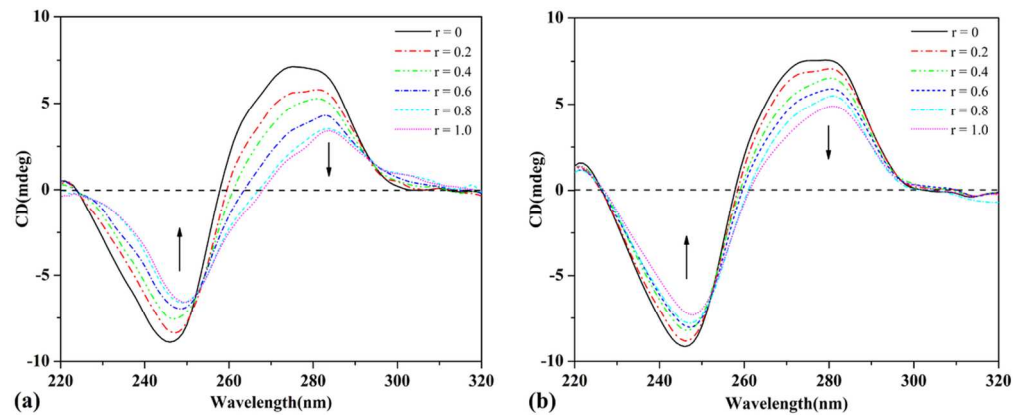
57x31mm (600 x 600 DPI)



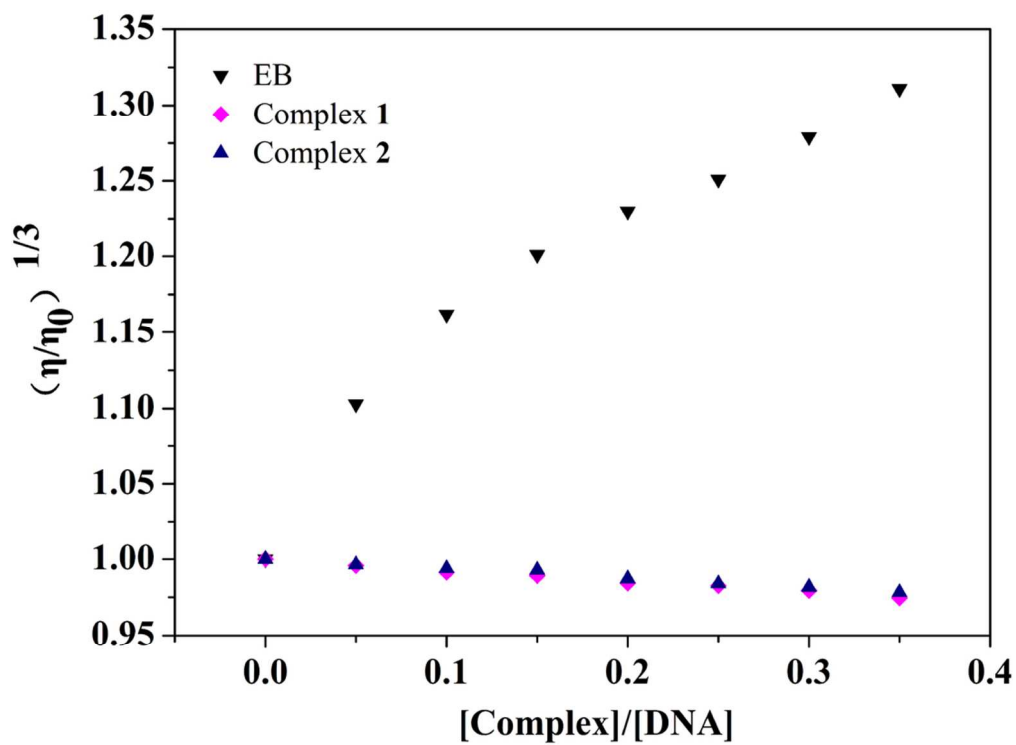
46x16mm (600 x 600 DPI)



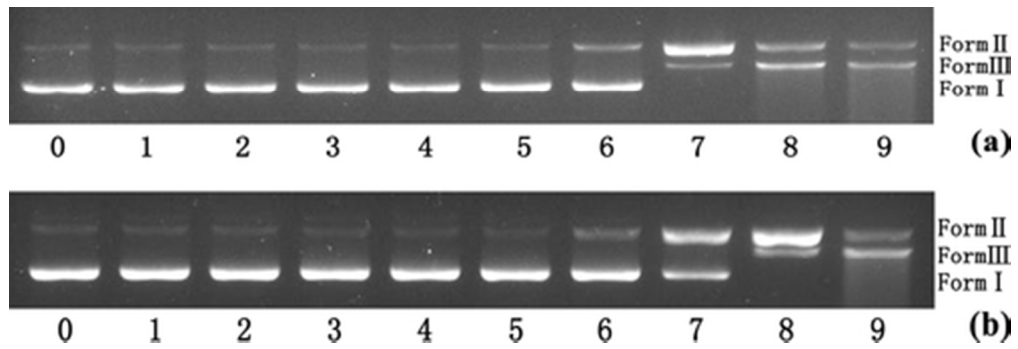
37x9mm (600 x 600 DPI)



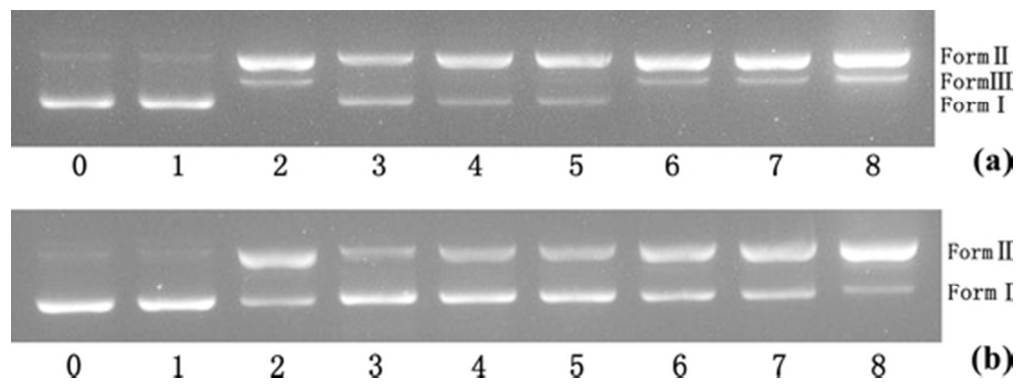
51x20mm (600 x 600 DPI)



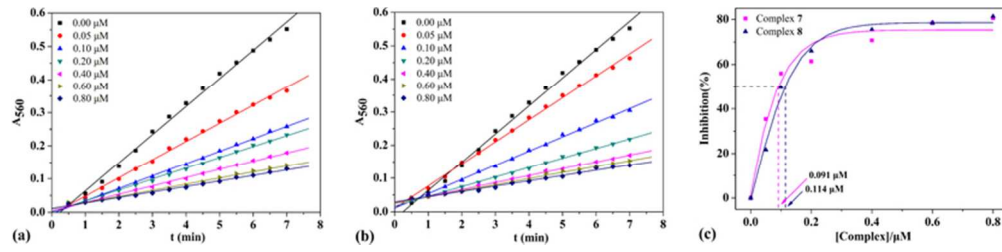
46x34mm (600 x 600 DPI)



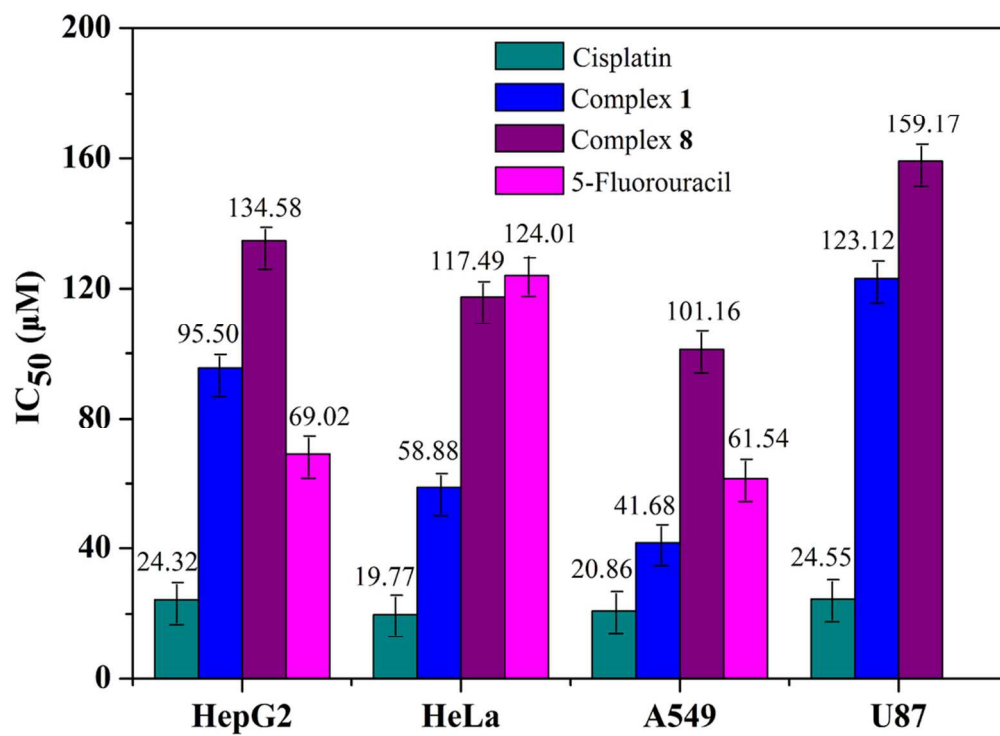
21x7mm (600 x 600 DPI)



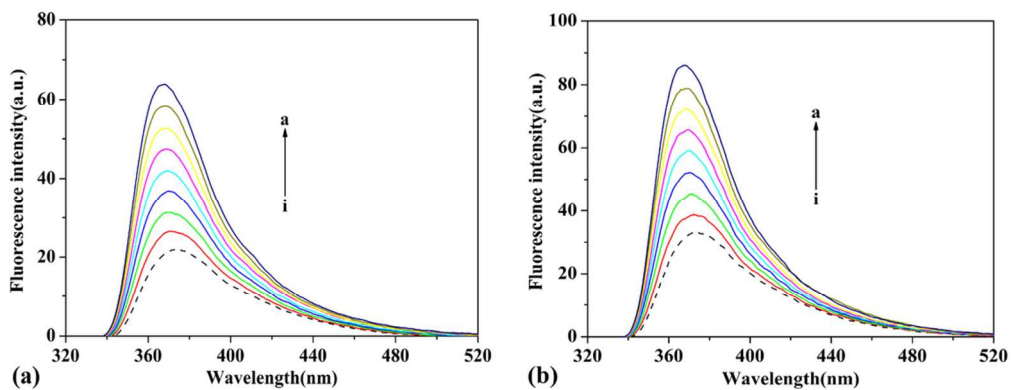
23x8mm (600 x 600 DPI)



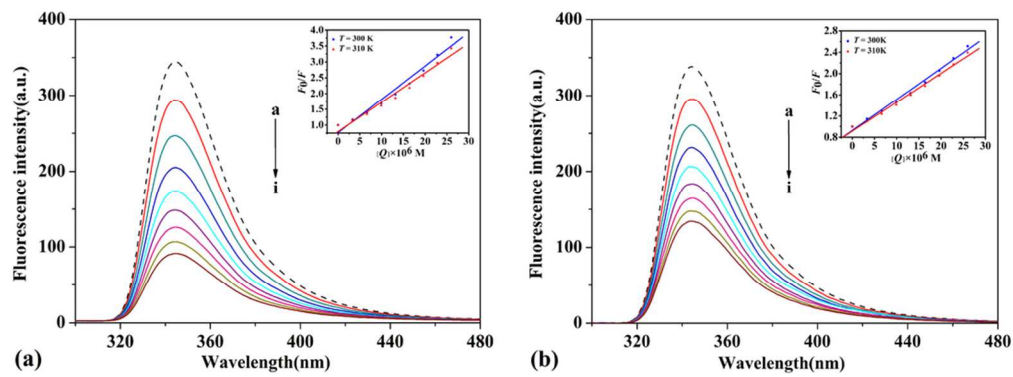
35x8mm (600 x 600 DPI)



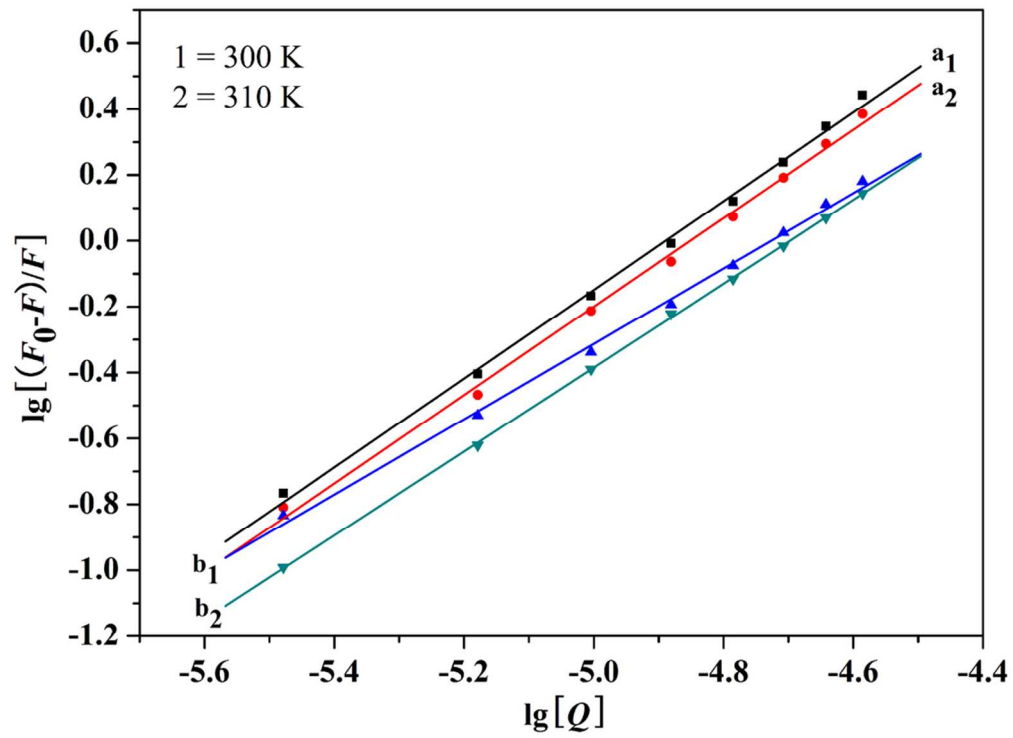
46x33mm (600 x 600 DPI)



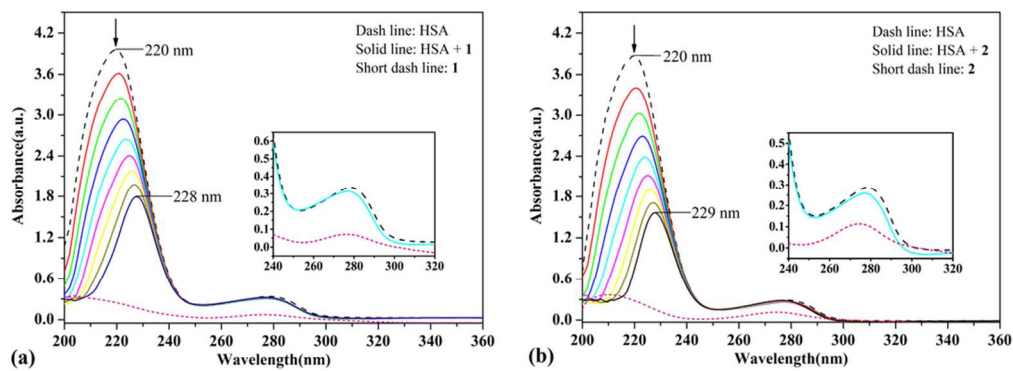
48x18mm (600 x 600 DPI)



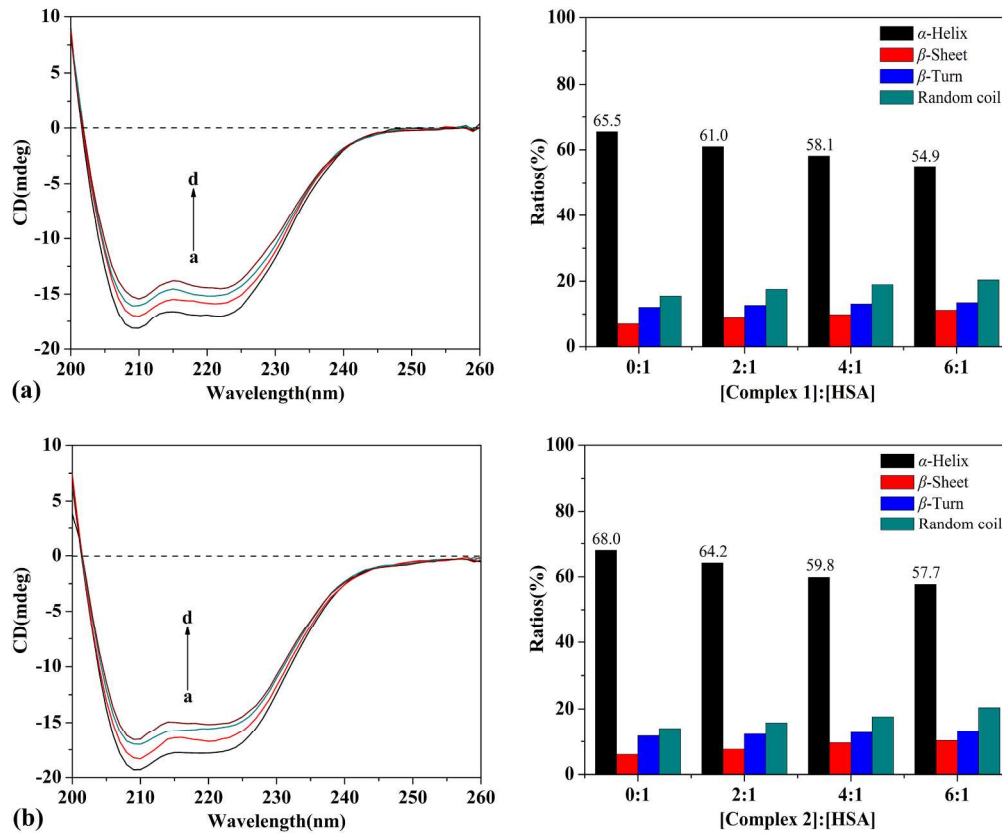
46x16mm (600 x 600 DPI)



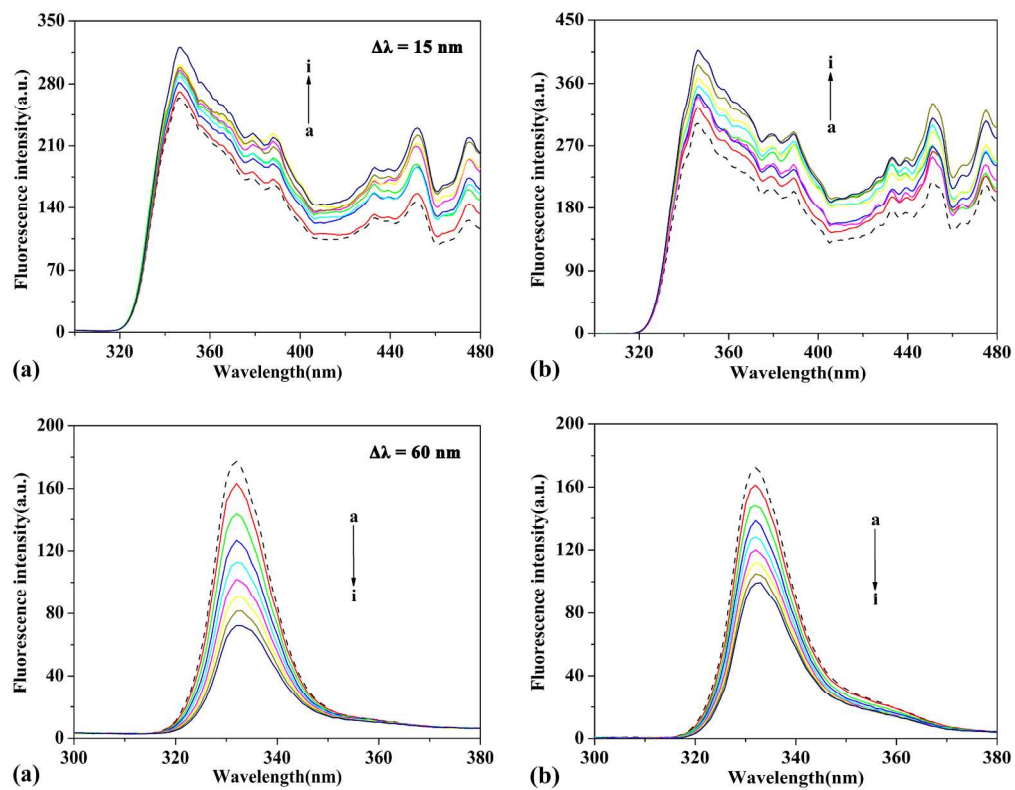
46x34mm (600 x 600 DPI)



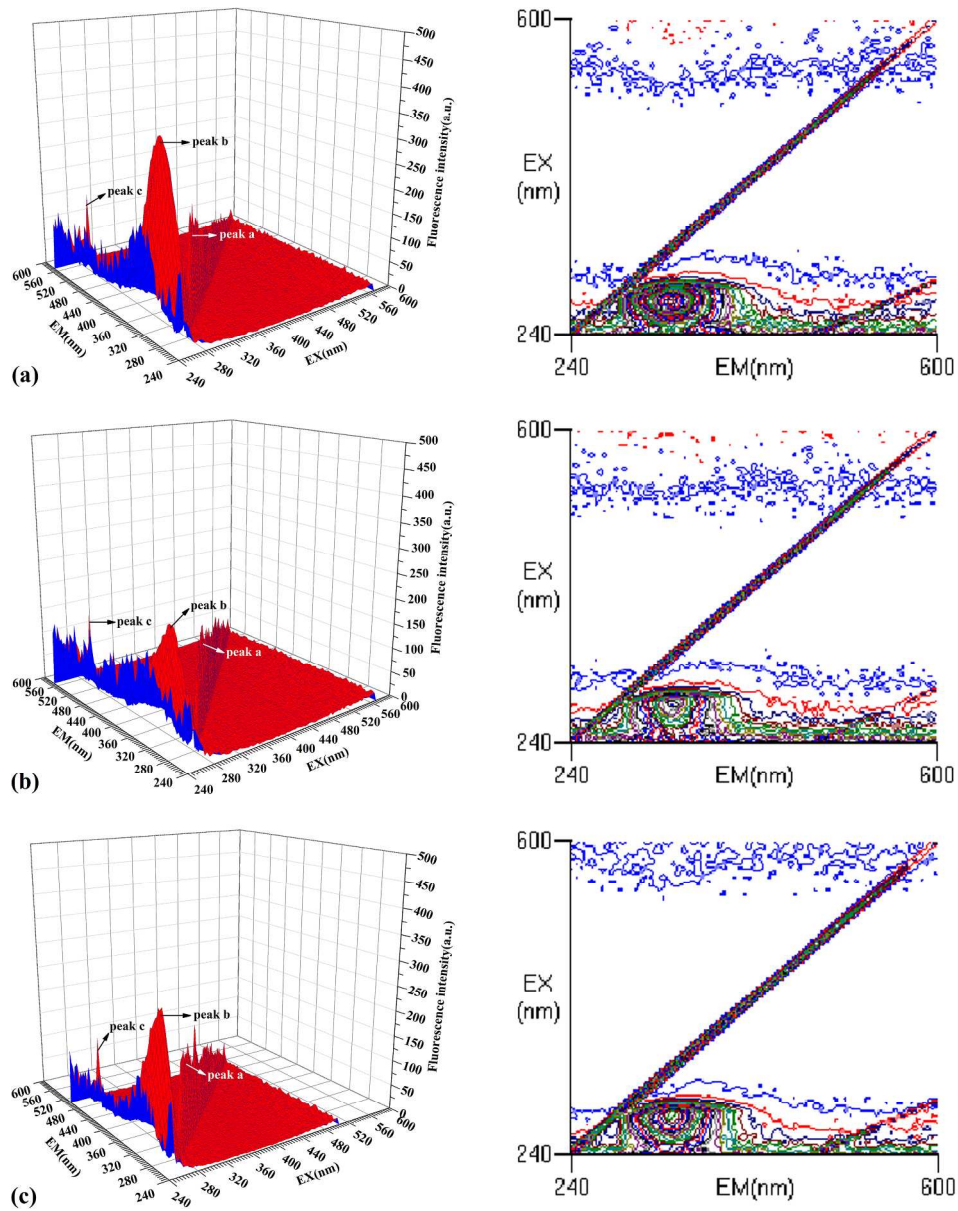
45x16mm (600 x 600 DPI)



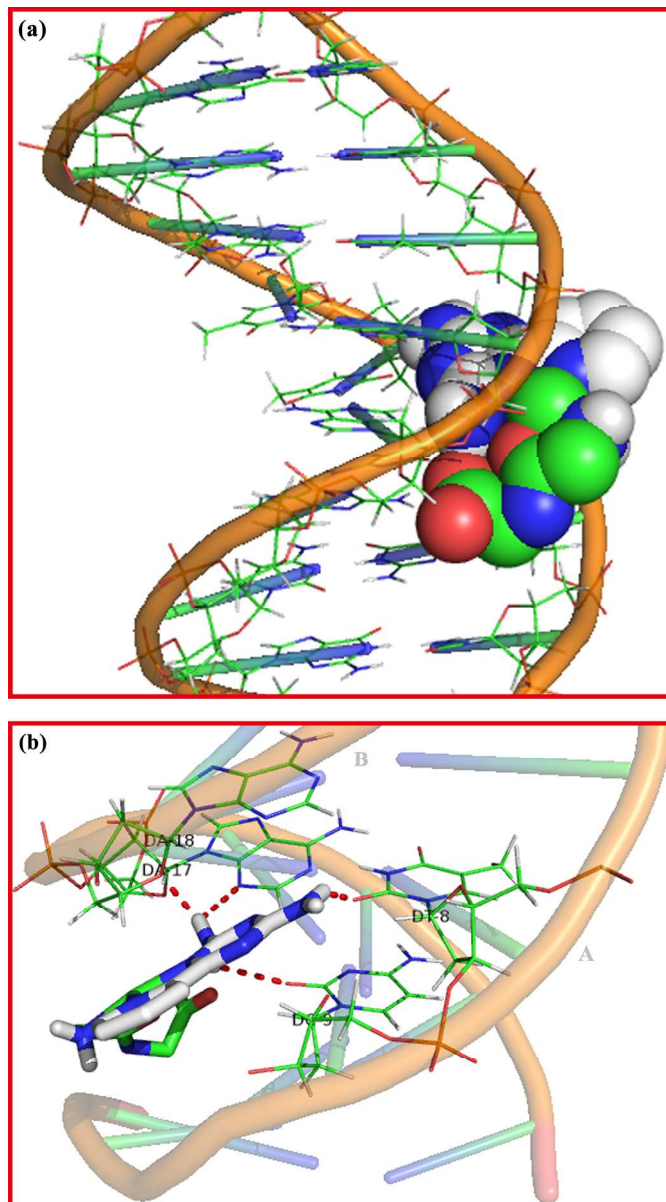
104x86mm (600 x 600 DPI)



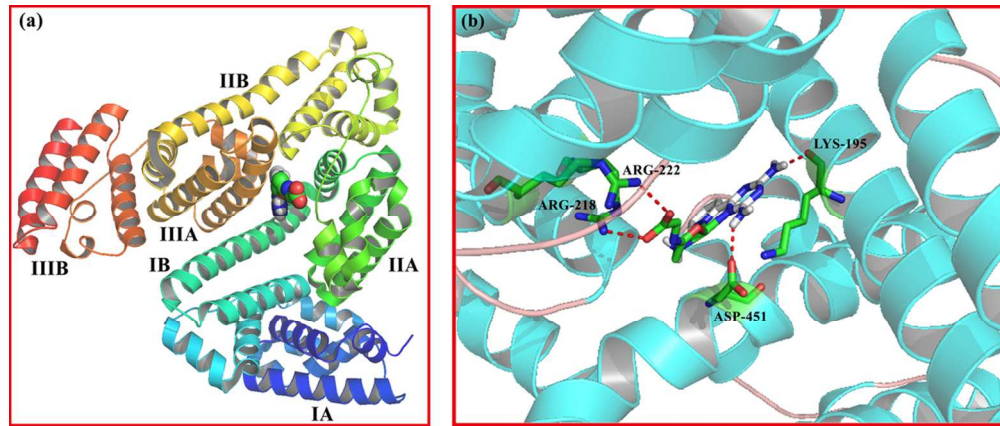
98x77mm (600 x 600 DPI)



133x169mm (600 x 600 DPI)



94x169mm (600 x 600 DPI)



53x22mm (600 x 600 DPI)